

Wilfrid Laurier University

Scholars Commons @ Laurier

---

Theses and Dissertations (Comprehensive)

---

2019

## THE EFFECT OF LOADING RATE ON ANNULUS FIBROSUS STRENGTH FOLLOWING ENDPLATE FRACTURE

John McMorran  
mcmo9620@mylaurier.ca

Follow this and additional works at: <https://scholars.wlu.ca/etd>



Part of the [Biomechanics Commons](#)

---

### Recommended Citation

McMorran, John, "THE EFFECT OF LOADING RATE ON ANNULUS FIBROSUS STRENGTH FOLLOWING ENDPLATE FRACTURE" (2019). *Theses and Dissertations (Comprehensive)*. 2182.  
<https://scholars.wlu.ca/etd/2182>

This Thesis is brought to you for free and open access by Scholars Commons @ Laurier. It has been accepted for inclusion in Theses and Dissertations (Comprehensive) by an authorized administrator of Scholars Commons @ Laurier. For more information, please contact [scholarscommons@wlu.ca](mailto:scholarscommons@wlu.ca).

THE EFFECT OF LOADING RATE ON ANNULUS FIBROSUS STRENGTH FOLLOWING  
ENDPLATE FRACTURE

John McMorran

Under the supervision of

Dr. Diane Gregory

Submitted to the Department of Kinesiology and Physical Education in accordance with  
requirements for the degree of Master of Kinesiology

Wilfrid Laurier University

© John McMorran, 2019

## ENDPLATE FRACTURE

**i. Abstract**

Low back pain is the most prevalent cause of chronic pain for North Americans, and its correlation with endplate damage, and deficient mechanical properties in the annulus fibrosus (AF) makes this injury particularly concerning. To date, biomechanical alterations in the AF following endplate fracture have not been well described. Owing to the AF's collagenous composition, and the intrinsic biomechanics of intervertebral discs (IVDs) during compression, it was hypothesized that the mechanical properties of AF specimens would show rate-dependent alterations in their tensile and adhesive strengths following endplate fracture. The purpose of the present study was to quantify the mechanical properties of the AF from IVDs that had sustained endplate fracture via different rates of applied compression. Porcine cervical spines acquired from a common source were stored at  $-20^{\circ}\text{C}$  until the night before testing at which they were left to thaw at room temperature. Specimens were dissected into functional spinal units (vertebra-disc-vertebra) at the levels C3/4 and C5/6. Segments were preconditioned with 300N of compressive force for 15 minutes using a uniaxial electromechanical material testing system. Following preconditioning, functional spinal units were compressed until fracture under displacement control at one of three loading rates: 15mm/s (fast), 1.5mm/s (medium), or 0.15mm/s (slow). Following fracture, two samples dissected from the AF were mechanically tested from each disc: 1) Bilayer samples were tested in tension at 1%/s to 50% strain; 2) multilayer samples were tested using a  $180^{\circ}$  peel test configuration at 0.5mm/s. Mechanical properties were compared with a 2-way analysis of variance and Tukey-Kramer post-hoc analyses. Results indicated significant differences in the compressive strength and stiffness of fast and medium-compressed functional spinal units compared to those compressed at the

## ENDPLATE FRACTURE

slowest rate of velocity. However, at the AF tissue-level, the present experiment did not detect alterations in mechanical properties stemming from different rates of endplate-fracture velocity. Previous work has shown that rapid internal intervertebral disc pressurization resulted in endplate fracture, along with decreased adhesion strength in these AF specimens compared to non-pressurized/non-fractured controls. While at the whole-disc level, the present experiment reports quantifiable differences in the strength and stiffness of functional spinal units, it is likely that velocities of compression were much too slow to incur the previously documented mechanism of decreased adhesion strength. Future research should seek to investigate a compressive model of endplate injury at high rates of velocity commensurate with falls from height or motor vehicle accidents.

**ii. Acknowledgements**

My first acknowledgement is to Dr. Gregory, as her mentorship gave me every opportunity to succeed. My second acknowledgement goes to my labmates, Derek, Sara, Mitch, and Rujavi, as their positivity and enthusiasm were a constant source of motivation. Finally, eternal thanks to my parents, John and Wendy, for their unwavering support, encouragement, and love.

**Table of Contents**

<b>i. Abstract.....</b>	<b>2</b>
<b>ii. Acknowledgements.....</b>	<b>4</b>
<b>iii. List of Abbreviations.....</b>	<b>8</b>
<b>iv. List of Figures.....</b>	<b>9</b>
<b>v. List of Tables.....</b>	<b>11</b>
<b>1. Introduction.....</b>	<b>12</b>
<b>1.1. Anatomy.....</b>	<b>13</b>
<b>1.1.1. Nucleus Pulposus.....</b>	<b>13</b>
<b>1.1.2. Annulus Fibrosus.....</b>	<b>15</b>
<b>1.1.3. Endplates.....</b>	<b>18</b>
<b>1.1.4. Vertebrae.....</b>	<b>22</b>
<b>1.2. Biomechanics.....</b>	<b>23</b>
<b>1.2.1. Biomechanics of the Intervertebral Disc during Axial Compression.....</b>	<b>23</b>
<b>1.2.2. Proposed Response of the Functional Spinal Unit during High Velocity         Compression.....</b>	<b>25</b>
<b>2. Purpose.....</b>	<b>28</b>

ENDPLATE FRACTURE

**2.1. Objectives.....29**

**2.2. Hypotheses.....30**

**3. Methods.....31**

**3.1. Functional Spinal Unit Specimens.....31**

**3.2. Geometry of IVDs.....33**

**3.3. Mechanical testing.....35**

**3.3.1. FSU Preconditioning and Experimental Conditions.....35**

**3.3.2. Tensile testing of the AF.....37**

**3.3.3. Lamellar Adhesion Test .....39**

**3.4. Data Analysis.....41**

**3.4.1. Compression-to-failure Analysis.....41**

**3.4.2. Tensile Strength Analysis- Bilayer AF samples.....43**

**3.4.3. Lamellar Adhesion Analysis- Peel Test samples.....45**

**3.5. Histological Procedure.....46**

**3.6. Statistical Analysis.....48**

**4. Results.....49**

**4.1. Endplate Fracture Morphology.....49**

<b>4.2. Compression-to-failure.....</b>	<b>52</b>
<b>4.3. Bilayer Tensile Test.....</b>	<b>55</b>
<b>4.4. Lamellar Adhesion Test.....</b>	<b>57</b>
<b>4.5. Histology.....</b>	<b>59</b>
<b>5. Discussion.....</b>	<b>61</b>
<b>5.1. Revisiting Objectives.....</b>	<b>68</b>
<b>5.2. Revisiting Hypotheses.....</b>	<b>70</b>
<b>6. Limitations.....</b>	<b>72</b>
<b>7. Conclusions.....</b>	<b>75</b>
<b>8. References.....</b>	<b>76</b>

**iii. List of Abbreviations**

**AF- Annulus Fibrosus**

**DDD- Degenerative Disc Disease**

**EP- Endplate**

**FSU- Functional Spinal Unit**

**IAF- Inner Annulus Fibrosus**

**IVD- Intervertebral Disc**

**LBP- Low Back Pain**

**NP- Nucleus Pulposus**

**OAF- Outer Annulus Fibrosus**

## ENDPLATE FRACTURE

**iv. List of Figures**

<b>Figure 1. Transverse section of intervertebral disc illustrating the NP and AF.....</b>	<b>14</b>
<b>Figure 2. Fiber orientations of lamellae.....</b>	<b>15</b>
<b>Figure 3. Inner and outer regions of AF.....</b>	<b>17</b>
<b>Figure 4. Sagittal view of EPs.....</b>	<b>18</b>
<b>Figure 5. EP fracture of apophyseal plate of porcine FSU.....</b>	<b>19</b>
<b>Figure 6. Hydrated cylinder model of NP and AF interplay during compression.....</b>	<b>24</b>
<b>Figure 7. EP surface area measurements.....</b>	<b>34</b>
<b>Figure 8. AF specimen mounting on tungsten rakes.....</b>	<b>37</b>
<b>Figure 9. Specimen mounting for 180° peel test.....</b>	<b>39</b>
<b>Figure 10. Compression-to-failure variables of interest.....</b>	<b>42</b>
<b>Figure 11. Bilayer tensile test variables of interest.....</b>	<b>44</b>
<b>Figure 12. 180° peel test plateau region.....</b>	<b>45</b>
<b>Figure 13. Histological sections of bovine caudal AF.....</b>	<b>47</b>
<b>Figure 14. EP Fracture Morphology.....</b>	<b>50</b>
<b>Figure 15. Slow-compression sub-fracture events.....</b>	<b>51</b>
<b>Figure 16. Ultimate strength results by rate.....</b>	<b>52</b>

ENDPLATE FRACTURE

**Figure 17. Stiffness results by rate.....53**

**Figure 18. Histological specimens (a-d).....60**

**Figure 19. Lamellar adhesion strength comparison with Snow et al. (2018).....64**

**Figure 20. Human lumbar and porcine cervical IVDs.....74**

**v. List of Tables**

**Table 1. Variables of interest for compression-to-failure, tensile, and 180° peel tests.....48**

**Table 2. Compression-to-failure.....54**

**Table 3. Bilayer tensile test.....56**

**Table 4. Lamellar Adhesion test.....57**

## 1. Introduction

Both in Canada and globally, low back pain (LBP) enacts a massive societal burden (Rapoport, Jacobs, Bell, & Klarenbach, 2004) due to the extensive medical costs (Merkhens et al., 2012), missed days of work (Dagenais, Caro, & Haldeman, 2008), and personal suffering associated with this condition (Vos et al., 2012). While pain has been documented to arise from injury to numerous spinal structures, mounting evidence suggests that degenerative disc disease (DDD) plays a pivotal role in the aetiology of LBP (Cassinelli & Kang, 2000). Though the mechanism by which endplate (EP) fracture impacts the intervertebral disc (IVD) is unknown, people who have suffered EP fracture seem predisposed to developing DDD (Fields, Ballatori, Liebenberg, & Lotz, 2018, Dudli, Haschtmann, & Ferguson, 2012, and Hadjipavlou et al., 2008). The majority of past research has focused on the morphological presence of EP fracture as the defining factor in DDD's initiation. Interestingly, a recent experiment by Snow et al. (2018) demonstrated that forces experienced during an EP fracture seem to have a large influence on subsequent IVD mechanics. However, Snow et al. (2018) utilized rapid internal pressurization to damage their specimens' EPs, and as such, it remains unclear as to whether lower rates of compression more comparable to those experienced in vivo might elicit similar alterations. Therefore, the purpose of the present study was to investigate the relationship between EP fractures at different rates of compression and subsequent alterations in the mechanical properties of the IVD.

## **1.1. Anatomy**

### **1.1.1. Nucleus Pulposus**

The nucleus pulposus (NP) articulates with the endplates of the superior and inferior vertebrae and is held in the centre of the IVD by the surrounding annulus fibrosus (Figure 1 and section 1.1.2). NP tissue is comprised predominantly of type II collagen and proteoglycans, and Cassinelli and Kang (2000) describe that for young human IVDs, 50% of their dry weight is comprised of proteoglycans. The viscoelastic properties of the NP are dictated by notochordal cells whose primary function is water retention. More numerous notochordal cells within an IVD permits greater hydrophilicity to tissue, but gradual extinction in the volume of notochordal cells over the human lifespan results in less hydrated, more fibrotic NP, compromising its biomechanical ability to withstand compression later in life (Murakami et al., 2010, Roughley, Alini, & Antoniou, 2002, Cassinelli & Kang, 2000, Antoniou et al., 1996).

In addition to variations in hydration over the lifespan, water retention in the NP is sensitive to daily activities, and the pressure gradients thereby imposed on the lumbar spine (Malko, Hutton, & Fajman, 1999). Farrell and Riches (2012) sought to quantify the Poisson's ratio of the NP and reported a positive relationship between increased amplitude of compressive force and radial bulging of the IVD. However, it was also reported that the more lateral bulging that occurred in IVDs, the greater their resistance to continued lateral bulging. This indicates that the NP's response to compression is nonlinear, and that the mechanical response of the tissue varies in conjunction with the amplitude of force application.

## ENDPLATE FRACTURE

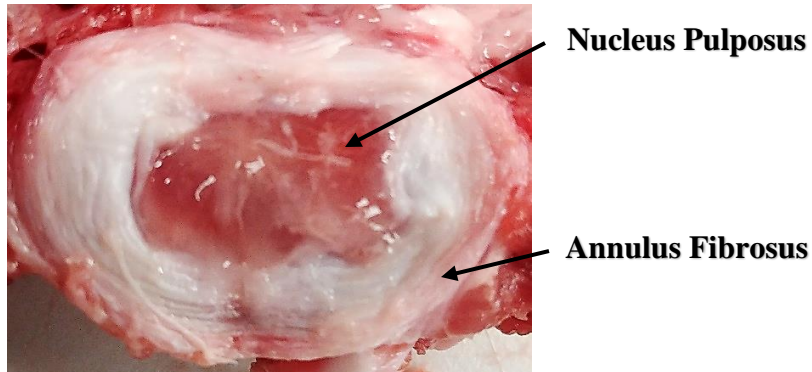


**Figure 1. Superior (axial) view of porcine intervertebral disc denoting the nucleus pulposus (NP) and annulus fibrosus (AF).**

Over the human lifespan (and the lifespan of certain mammals), losses in NP notochordal cell volume results in a stiffer, less hydrated NP. Due to the mechanics of EP fracture, evidence suggests that aging's natural reduction in notochordal cells makes EP fracture less likely later in life, while herniation of the NP and/or tearing of the AF seem more prevalent with increased age (Cheung et al., 2009).

### 1.1.2. Annulus Fibrosus

The annulus fibrosus (AF) is a ring-like substructure of the IVD comprised of 15-25 circumferentially-wrapped layers (lamellae) of tissue. Lamellar fiber angles vary from 19 to 50 degrees relative to the transverse plane (Elliot, 1999)- as demonstrated by Figure 2- while adjacent sheets are orthogonally aligned at approximately 60 degrees (Elliot, 1999). Lamellar fibres insert into the superior and inferior cartilaginous EPs of articulating vertebrae, anchoring the structure to both of its articulating EPs. However, structural and functional differences between sub-sections of the AF, specifically the inner and outer AF (IAF and OAF, respectively) necessitate division between these regions.

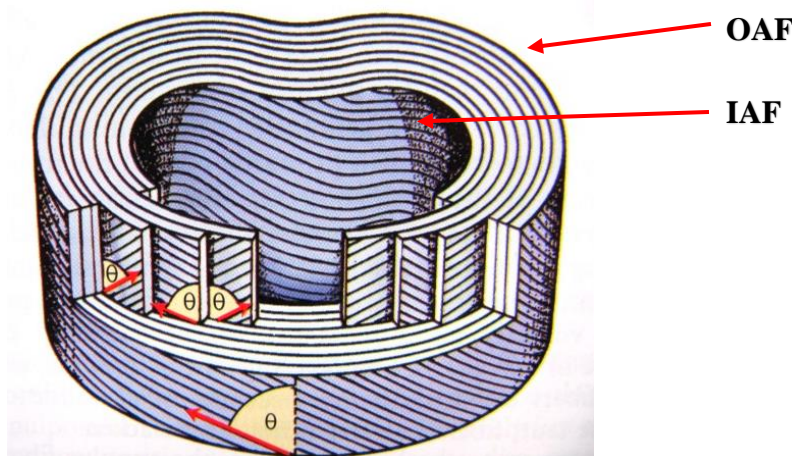


**Figure 2. Fiber orientations of adjacent lamellar sheets in the human annulus fibrosus.**

**Image obtained from Adams et al. (2010).**

## ENDPLATE FRACTURE

Most proximal to the NP (Figure 3), the IAF maintains a lamellar structure, although layers located here are more often incomplete, and sometimes difficult to differentiate (Fujita, Wagner, Biviji, Duncan, & Lotz, 2000). IAF cells are visually distinct from their OAF counterparts as well, because IAF cells more closely resemble the spherical cells ‘packed’ in the NP, than the long fusiform cells of the OAF (Setton and Chen, 2004, and Bruhlmann et al., 2002). During a profilometry examination of the IVD, Adams, McNally, and Dolan (1996) observed the fluid-like mechanical response of the NP to extending well into the IAF, and this complementarity in function, combined with the IAF’s abundance of proteoglycans (the glycosylated proteins formed by notochordal cells) and type II collagen, appear to make this structure better suited to resist axial compression than tensile deformation (Li, Liu, Guo, Yang, & Li, 2014).

Conversely, the OAF (Figure 3) exhibits distinct partitions between lamellae, and the type I collagen fibres that predominate in this region are poorly hydrated, resulting in a stiff, fibrous structure. Owing to its multilayered, laminate configuration, neighbouring AF plies adhere via the interlamellar matrix; a viscid extracellular matrix whose composition of proteoglycans, type VI collagen, and elastin provide its adhesive and elastic properties (Gregory, Bae, Sah & Masuda, 2012, Melrose et al., 2008). Delamination between neighbouring lamellae has demonstrated circumferential tearing of the AF, illustrating that both damage to AF fibers, or loss of lamellar adhesion may result in annular dysfunction. Gregory, Bae, Sah, and Masuda (2012) extracted samples from the OAF and IAF to examine the strength of the interlamellar matrix in these two regions, and their investigation reported that samples extracted from the OAF were 33% stronger than samples extracted from the IAF. The greater stiffness and strength of the fibers and interlamellar matrix of the OAF may be a product of this region’s improved fibrillar

## ENDPLATE FRACTURE

organization, or superior adaptation to tensile strain. The AF's sub-regions create a complex architecture within the IVD, and the individual and combined biomechanical properties of each region appear critical to adequate function and health.

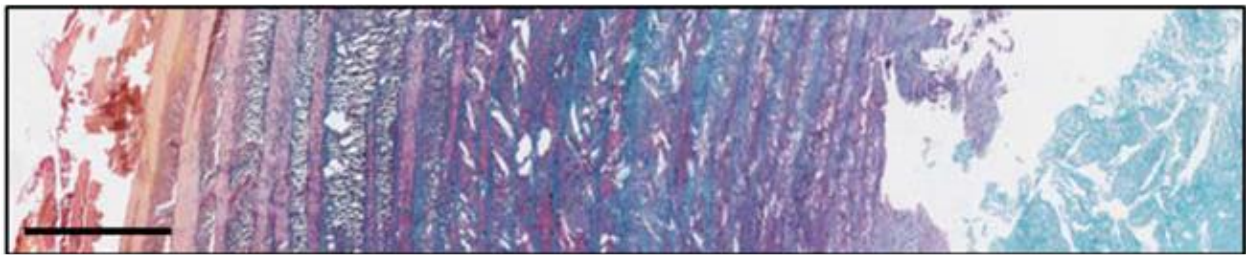
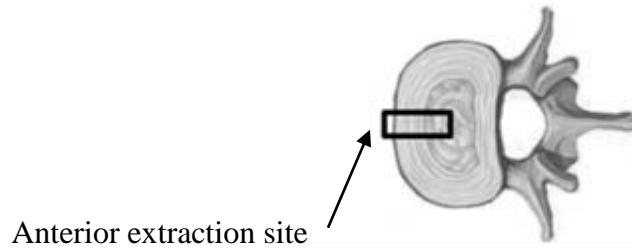


**Figure 3. Porcine lumbar tissue treated with a combination stain (Weigert's hematoxylin, picrosirius red, alcian blue) to demonstrate the gradient distribution of proteoglycans (stained blue) and collagen (stained red) throughout the IVD. The left-hand side of the figure is the OAF, while the right-hand side is the NP. Image obtained from Monaco, DeWitte-Orr, and Gregory (2016).**

### 1.1.3. Endplates

Human EPs are comprised of a thin layer of hyaline cartilage overlaying the slightly concaved articulating surfaces of vertebrae (Figure 4). The purpose of EP hyaline cartilage is twofold: 1) to anchor fibres of the AF, connecting the AF to the superior and inferior vertebrae (Rodrigues, Thambyah, & Broom, 2017); 2) the fluctuating pressure gradients associated with daily human activities result in the diffusion of water and metabolites across this porous barrier, thereby permitting this influx from vertebrae into NP and IAF tissue (Cassinelli & Kang, 2000).

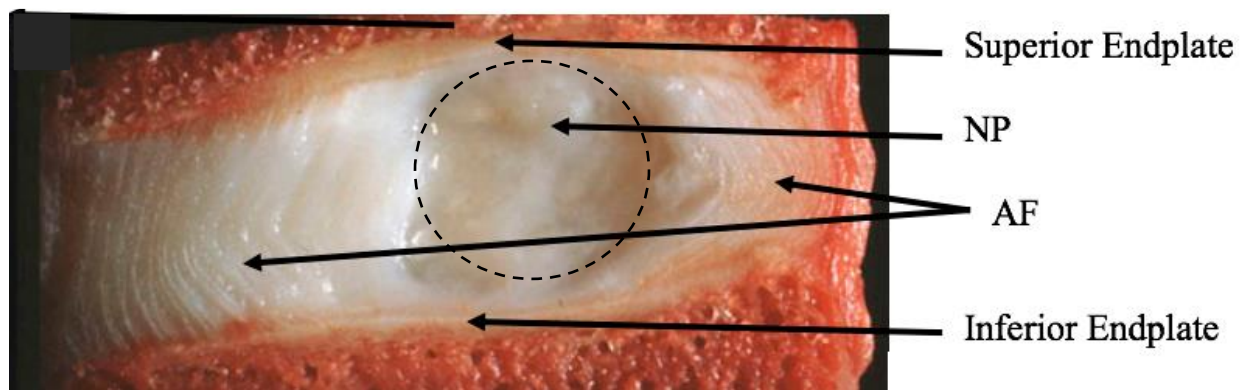


**Figure 4. Sagittal view of IVD demonstrating the superior and inferior EPs along with the NP and AF. Image obtained from Adams et al. (2010).**

Although axial compression is responsible for EP diffusion, supraphysiological axial compression can damage the EP and/or vertebra. Aufdermaur (1974), and Karlsson, Lundin, Ekström, Hansson, and Swärd (1998) discovered that in juveniles, the EP is the weakest structure of the functional spine unit (FSU; vertebra-IVD-vertebra) during axial compression, and this trend that appears consistent with other mammals, including porcine cervical specimens (Lundin,

## ENDPLATE FRACTURE

Ekstrom, Hellstrom, Holm, and Sward, 2000; Lundin et al., 1998). Furthermore, EPs exhibit predictable patterns of failure wherein the apophyseal ring that demarcates the horizontal growth plate is the region most likely to fracture (Allan et al., 2005, Lundin, Ekstrom, Hellstrom, Holm, & Sward, 2000, Lundin, Ekstrom, Hellstrom, Holm, & Sward, 1998, Karlsson, Lundin, Ekstrom, Hansson, Sward, 1998, and Aufdermaur, 1974). This region's vulnerability stems from the delay in the calcification of its articular cartilage to allow for transverse expansion during growth (Adams, Bogduk, Burton, & Dolan, 2012). Figure 5 illustrates an EP fracture along the posterior apophyseal ring of a porcine cervical specimen.

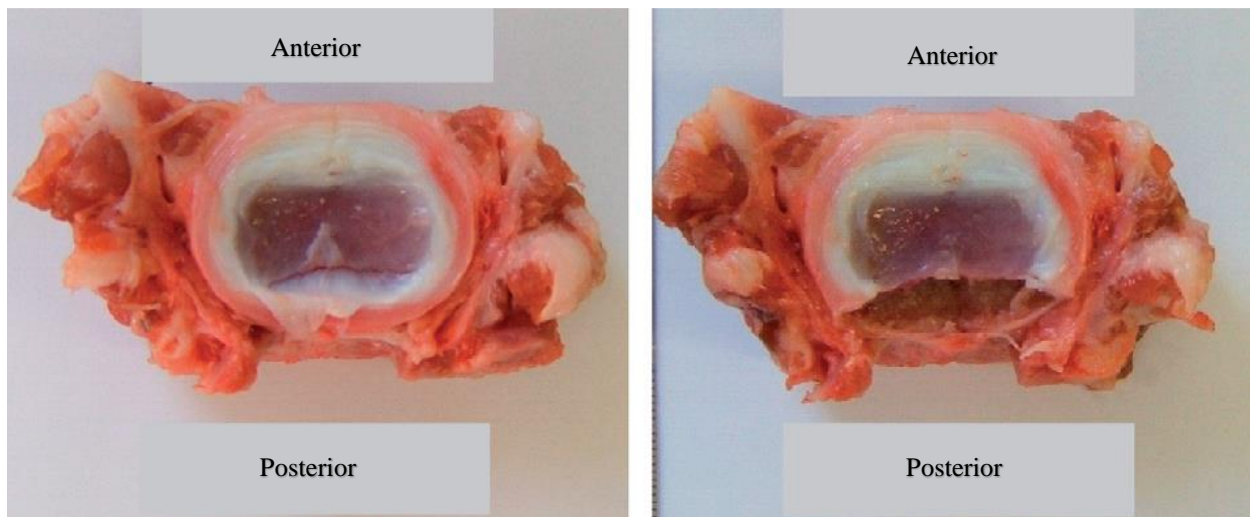


**Figure 5. Inferior vertebra from a porcine FSU that failed via EP fracture along the posterior margin of its apophyseal plate. Image on the right demonstrates depth of fracture and injury as bony fragments of specimen (left) were removed. Image obtained from Brown, Gregory, and McGill (2008).**

## ENDPLATE FRACTURE

Due to the vulnerability of the EP in conditions of axial loading, some researchers posit that EP fracture is the most impactful mechanical disruption that can occur to the spine (Dudli, Haschtmann, & Ferguson, 2012). In a study examining stress distributions during compression of the FSU, Przybyla, Pollintine, Bedzinski, and Adams (2006) applied up to 2kN of axial compression to human cadaveric FSUs in neutral, slightly flexed, and slightly extended positions. They found that when EP fracture occurred, intradiscal pressure decreased by 37%, and the maximum stresses experienced by the anterior AF were decreased by 24%, while there was an increase of 93% of the stress placed on the posterior AF. Additionally, when examining the stress profiles of IVDs, Adams et al. (1996) observed that EP damage decreased the pressure in fracture-adjacent IVDs by 57%. Results like those observed by Przybyla et al. (2006) and Adams et al. (1996) suggest that EP fracture typically occurs prior to annular disruption, and that it is EP injury and not annular damage, that dictates the altered stress displacements that can affect one or more levels of the spine.

While the correlation between EP injury and AF dysfunction is incomplete, sclerotic deposits in the EP are believed to develop in response to mechanical trauma (Dudli, Haschtmann, & Ferguson, 2012), and increased EP sclerosis has been observed with more severely degenerated IVDs (Pye et al., 2007). These calcified deposits may inhibit EP diffusion (either directly, or due to diminished vertebral-capillary function, Rodriguez et al., 2012) to the extent that cells within the IVD no longer receive adequate hydration and nutrition, resulting in apoptosis of nutrition-starved cells. Sufficient cellular death can cause focal disruptions in the NP or AF which can result in altered biomechanics of one or more spinal segments (Adams, McNally, &

Dolan, 1996), increased inflammation, and ultimately the degenerative cascade characterized by DDD (Rodriguez et al., 2012, Stokes & Iatridis, 2004).

#### **1.1.4. Vertebrae**

Internally, the bulk of the vertebral body is composed of cancellous bone, and this considerable volume is encompassed by a thin, cylindrical shell of cortical bone. The honeycomb appearance of cancellous bone stems from its many vertical and horizontal bony pillars or trabeculae. The patterns of stress vertebrae experience in vivo has been shown to largely dictate the thickness and abundance of trabeculae in vertebrae. Elite weightlifters have been found to possess thicker and more abundant trabeculae throughout their vertebral bodies, permitting them to withstand far greater compressive forces than most other humans (Adams et al., 2012). Conversely, excessive thinning or weakening of trabeculae within vertebrae can result in an increased likelihood of fracture. Osteoporotic kyphosis is a condition where excessive catabolism of bone can result in microfracture of trabeculae in the anterior vertebral body, until such time that anterior collapse occurs. The stooped posture and comorbidities associated with osteoporotic kyphosis (Harrison, Siminoski, Vethanayagam & Majumdar, 2007) illustrate the importance of trabecular architecture to vertebral health and function. Bone-mineral density investigations agree that reduced bone volume more adversely affects vertebral trabeculae than cortical bone, due to the large surface area presented by this porous surface (Fields, et al., 2011). Furthermore, the acuity of bone-mineral density investigations has reached a juncture where persons most at-risk of vertebral fracture, and even sometimes vertebral fracture location, can be predicted with moderate prognostic success (Fields, et al., 2011).

## **1.2. Biomechanics**

### **1.2.1. Biomechanics of the intervertebral disc during axial compression**

For a healthy, undamaged IVD, excessive axial compression in the neutral posture will result in EP fracture (Hadjipavlou et al., 2008). Healthy IVDs are rich in proteoglycans and well-hydrated, so their NP and IAF display mechanical properties similar to those of an incompressible fluid (Fan, Ghista, Sridhar, & Ramakrishna, 2005). However, in response to axial compression, the NP deforms radially, while the ring of the IAF attempts to restrict this radial bulging (Figure 6). Confined within the nuclear cavity, pressure in the NP and IAF increases (Adams, McNally, & Dolan, 1996), resulting in the propagation of force through the IVD and onto the EPs where, with sufficient compressive insult, trabeculae within the vertebral body will collapse as the NP fractures and displaces the EP (Adams et al., 2012). Specifically, once compressive stresses rise above the ability of trabeculae to resist, the vertical columns of bone bend, and the shear forces created by these shifting and/or twisting columns cause initial fractures to occur in transversely-oriented trabeculae. Once transverse trabeculae fail the vertical, weight-bearing pillars of bone are no longer supported against buckling. As the EP fails, NP material forces its way into the vertebral body, and its degree of penetration, and the volume of NP material extruded are regulated by the amount of damage present in the internal architecture of the vertebra. For skeletally immature humans, the unossified apophyseal ring appears to create a cartilaginous ‘seam,’ which has been identified as the most prevalent region of failure (Brown, Gregory, and McGill, 2008).

## ENDPLATE FRACTURE

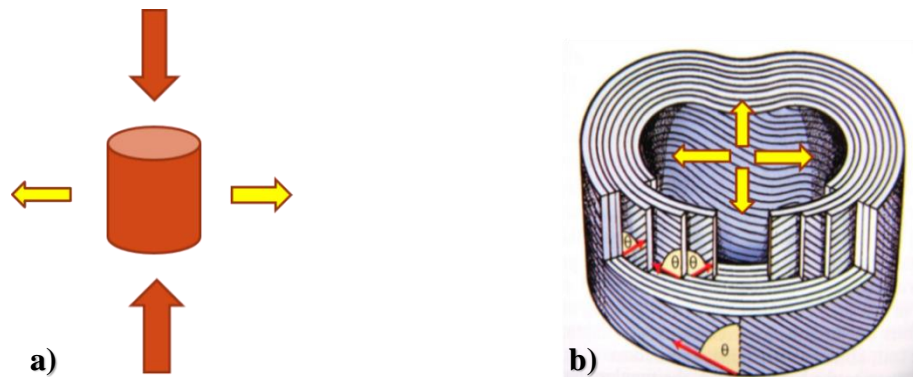


**Figure 6. Modelled as a hydrated cylinder, a) illustrates the radial expansion (yellow arrows) of the NP when compressed (red arrows), and b) demonstrates that the AF confines and resists this radial expansion. Image obtained from Adams et al. (2010).**

Pressurization of the NP during axial compression causes it to radially expand against the restrictive structure of the IAF, and confining this radial bulging results in outward propagation of tension through the IAF and OAF (Fan, Ghista, Sridhar, & Ramakrishna, 2005). This increase in pressure and resultant tensioning of the AF produces two biomechanical outcomes: 1) increased tension takes the crimp out of AF fibres, better preparing the OAF to handle strain (Fujita, Wagner, Biviji, Duncan & Lotz, 2000); and 2) increased intradiscal pressure improves AF resistance to axial compression, as the internal layers of the IAF play a vital role in withstanding axial loads (Adams, McNally, & Dolan, 1996).

### **1.2.2. Proposed response to high-velocity compression and EP fracture**

As discussed in section 1.2.1., the synergy between the NP and AF likely results in an AF that tensions at an equal rate to the NP's radial expansion.

A recent experiment conducted by Snow et al. (2018) examined the mechanical consequence of endplate fracture on the strength of the AF in porcine IVDs. The authors reported a 31% reduction in the AF annular adhesion strength of specimens that sustained EP fracture via a rapid internal pressurization mechanism, at a mean pressurization rate of 17.5MPa. The significant reduction in annular adhesion strength suggests some degree of failure to the extracellular matrix between layers of the AF following the rapid tensioning and recoil caused by the rapid increase in internal pressure and subsequent fracture, respectively.

The process reducing lamellae adhesion (delamination) is posited to initiate with unequal application of strain to oppositely-oriented, adjacent lamellae. Due to their complexity, the heterogeneity of stress distributions among even healthy IVDs are difficult to model and predict, and compressive forces are not equally distributed among AF tissue. Anatomical differences between sub-regions of the AF, along with the morphological characteristics of the segment, contribute to the stress response and distribution of forces within the IVD. During compression, the reduced distance between the superior and inferior vertebrae bend lamellar fiber directions toward a more transverse orientation (Adams et al., 2012), while radial forces simultaneously propagate through a tensioning AF. Therefore, during compression of the AF and the distinct responses of its sub-regions, if different relative deformations occur between adjacent lamellae, the interlamellar matrix may be damaged as plies 'slide' past one another, or contort in such a

## ENDPLATE FRACTURE

way as to strain the interlamellar matrix beyond its elastic capabilities. Such interlamellar sliding has been posited to initiate delamination between the annular layers (Gregory, Veldhuis, Horst, Brodland, & Callaghan, 2011).

Another mechanism posited to be responsible for annular weakening is the ‘buckling’ of the AF with depressurization of the NP following fracture. With compression, hydrostatic pressure in the NP increases until such a point that, in a young, hydrated IVD, the cranial EP will collapse. EP fracture permits nuclear material to invade the EP space, and this increase in volume in the closed, hydraulic system of the IVD results in depressurization of the NP, transferring an increased amount of the compressive load onto the AF (Przybyla, Pollintine, Bedzinski, & Adams, 2006, and Adams, Freeman, Morrison, Nelson, & Dolan, 2000). This increased load bearing by the AF can result in radial deformation of the AF where more peripheral lamellae (such as those in the OAF) bulge outward toward the perimeter of the IVD, and more proximal lamellae (such as those in the IAF) buckle inward toward the NP (Adams, Freeman, Morrison, Nelson, & Dolan, 2000). Chronic, excessive load-acceptance by the AF following dehydration, and a reduced NP height has been demonstrated to incite delamination and internal dysfunction of IVDs (Adams, Stefanakis & Dolan, 2010, and Adams, McNally, and Dolan, 1996), and may be a critical aetiological development in DDD (Adams, Stefanakis & Dolan, 2010, Di Martino, Vaccaro, Lee, Denaro, & Lim, 2005; Adams, McNally, and Dolan, 1996). However, the present study is concerned with the buckling mechanism in a more acute manner. It has been demonstrated that at increasing velocity, the NP stiffens and resists radial deformation to a greater degree (Farrell & Riches, 2012). Following EP fracture at faster speeds, the present study posits that the NP may not radially expand as much as it would during a slower compression.

## ENDPLATE FRACTURE

Therefore, the instant of EP fracture and depressurization, the AF is posited to be less prestrained when compression is transferred onto its structure, and therefore less capable of resisting buckling and deformations beyond the elastic limits of the interlamellar matrix.

While the exact mechanism of EP fracture and AF weakening has not yet been elucidated, evidence from Snow et al. (2018) indicates that internal hydraulic pressurization, and its rapid application of tension through the AF, may accentuate the injurious internal mechanics of the IVD that result in reductions in annular adhesion strength. EP fracture appears significantly related to dysfunction of the AF later in life (Dudli, Haschtmann & Ferguson, 2012), and due to the work conducted by Snow et al. (2018), the present thesis attempted to examine the sensitivity of the AF's mechanical properties to different velocities of EP fracture via compression.

## **2. Purpose**

The purpose of the present study was to investigate the effect of rate of compression on the mechanical properties of the AF following EP fracture. As discussed in section 1.2.2., velocity is believed to play a pivotal role in the mechanical characteristics expressed by the viscoelastic tissues of IVDs. However, knowledge regarding the impact of EP-fracture acquired without rapid pressurization of an FSU is currently lacking. As such, the results demonstrated by Snow et al. (2018) motivated three main objectives in the present study, by which the behaviour of FSUs and AF tissues were intended to be targeted via different rates of compression-to-failure.

## **2.1. Objectives**

- 1) to elicit different magnitudes of viscoelastic responses from FSUs compressed via different velocities of compression.
- 2) to create EP fracture in all of the FSUs that were compressed to failure, regardless of rate of compression.
- 3) to quantify the effect of different FSU compression velocities on AF mechanical properties.

## **2.2. Hypotheses for Mechanical Testing of FSU and AF specimens**

The viscoelastic response of IVDs, and the mechanical interplay of their sub-structures presented the basis for the present study's hypotheses. With regards to compression of whole FSUs, it was hypothesized that:

- 1) faster compression velocities would result in greater measures of ultimate strength and stiffness, and FSUs would displace less prior to EP fracture than those at slower compression velocities.
- 2) FSUs, regardless of rate of compression, would all sustain an EP fracture.

At the bilayer level it was hypothesized that:

- 1) EP fracture sustained at the fastest compression rate would result in a more compliant AF that would also reach lower stress magnitudes, and displace to a greater degree than samples compressed at the slowest compression rate.

In regards to AF peel strength, it was hypothesized that:

- 1) specimens compressed at the fastest velocity would have the lowest AF adhesion strengths and the greatest adhesion strength variability, compared to the slowest compression rate.

### **3. Methods**

#### **3.1. FSU Specimens**

The present study utilized 21 porcine cervical spines obtained from a common source in the Kitchener-Waterloo region. Animals were 6 months old at the time of slaughter, and their weight fluctuated between 100kg and 120kg. Once specimens were acquired from the common source, they were kept frozen at -20°C until use. Control for diet, weight, physical activity levels, previous injuries, and age made this study population highly homogeneous, however, as the ultimate goal is human transferability, human cadaveric tissue remains the gold-standard for in vitro experiments of this nature.

FSUs were excised from the spines at the C3/4 and C5/6 levels to utilize the most morphometrically similar specimens in the porcine cervical region as compared to human lumbar spines (Busscher, Ploegmakers, Verkerke & Veldhuizen, 2010, Yingling, Callaghan, & McGill, 1999, and Oxland, Panjabi, Southern, & Duranceau, 1991). Mechanical testing used 31 specimens, and 8 additional FSUs were utilized for histological examination. However, improper dissection of tissues resulted in 39 serviceable FSUs extracted from 21 porcine cervical spines.

Experimental group size was determined a priori based on the variance reported in similar mechanical testing work including Harvey-Burgess and Gregory (2019), Snow et al. (2018), and Gregory et al. (2009). For 80% power, a sample size of 10 per group was determined.

Prior to mechanical testing, specimens were removed from the freezer and thawed at room temperature overnight. Specimens were left to thaw for a minimum of 10 hours, and no longer than 16. Once thawed, two FSUs (C3/4 and C5/6) were removed from each spine and dissected

to their osteoligamentous components. FSUs were wrapped in gauze soaked with phosphate buffered saline (PBS) and plastic wrap, to ensure that they stayed hydrated during the loading protocol.

### 3.2. Geometry of Intervertebral Discs

Anterior-posterior, and medial-lateral EP width measurements were taken with digital calipers of the superior and inferior EPs of FSUs, and these measurements were averaged to estimate the EP size of tested specimens because, centred as they were in FSUs, tested EPs were inaccessible until post-fracture. Two anterior-posterior and two medial-lateral widths were taken for each specimen, and widths were averaged before values were applied to the following equation:

$$SA = \pi ab.$$

**SA** represents surface area of an ellipse, **a** represents the radius of the anterior-posterior width, and **b** represents the radius of the medial-lateral width. Force was normalized to specimen EP area by dividing ultimate force by specimen surface area. Expressing compressive values normalized to EP area permitted comparison across specimens, and provides a modest level of transferability to humans (Monaco, DeWitte-Orr, & Gregory, 2016, Busscher, Ploegmakers, Verkerke, & Veldhuizen, 2010, Beckstein, Sen, Schaer, Vresilovic, & Elliott, 2008, O'Connell, Vresilovic, & Elliott, 2007).

ENDPLATE FRACTURE

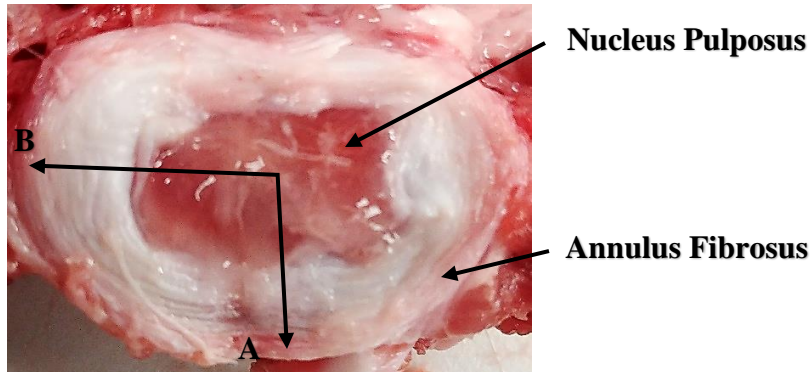


**Figure 7. Anterior-posterior (A) and medial-lateral (B) radiuses used to calculate EP surface area.**

### **3.3. Mechanical Testing**

#### **3.3.1. FSU Preconditioning and Experimental Conditions**

Prior to being randomly assigned to their experimental loading conditions, all specimens were preconditioned with 300N of axial compression in the neutral posture for 15 minutes using a uniaxial electromechanical material testing system (MTS, Eden Prairie, MN). The purpose of preconditioning was to rid samples of post-mortem swelling and any effects from freezing.

In an experiment performed by Azarnoosh et al (2017), porcine lumbar segments frozen to -20°C and -80°C demonstrated decreased specimen stiffness compared to fresh controls, and a similar finding was reported by Callaghan and McGill (1995) who found a 24% increase in the compressive load, and 33% increase in energy absorbed by frozen porcine cervical FSUs compressed to failure, compared to unfrozen controls. Conversely, Dhillon, Bass, and Lotz (2001) reported no effect on the elastic or creep response of human cadaveric IVDs compared to frozen counterparts. Clearly, in vivo tissue responses cannot be perfectly modelled by frozen specimens, but if the mechanical effects of freezing are taken into account, porcine specimens have been demonstrated as a suitable analog in lieu of fresh human tissue.

Following preconditioning, each FSU was compressed to failure in the axial direction at one of three loading rates: 0.15mm/s, 1.5mm/s, and 15mm/s (randomly assigned). The material testing system was limited to a maximum speed of 17mm/s. To improve consistency, 15mm/s was selected as the fastest compression rate, and the medium and slow compression rates were selected to be slower by a magnitude of 10 times, resulting in compression rates of 15mm/s, 1.5mm/s, and 0.15mm/s respectively. All specimens were free-mounted between the actuator

ENDPLATE FRACTURE

heads of the uniaxial electromechanical material testing system, then compressed until audible fracture of the specimen occurred.

### 3.3.2. Tensile Testing of the AF

In order to access the posterior OAF, posterior elements of the FSU were removed with a handsaw before superficial samples of OAF were extracted. Bilayer (2-4 layers) AF samples were then carefully dissected from the OAF under an Axiolab microscope (Zeiss, Jena, Germany). Following dissection, sample thickness was measured with a laser displacement sensor (IL-065, Keyence, Mississauga, ON). Specimens were then mounted onto 0.7mm spaced tungsten rakes in a biaxial mechanical testing apparatus (Biotester, Cellscale, Waterloo, ON).

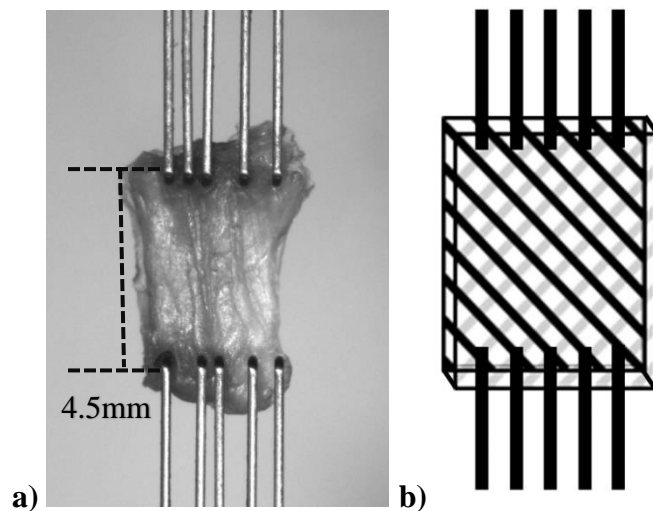


**Figure 8. Superficial OAF bilayer specimen mounted on tungsten rakes (a) while graphic (b) illustrates the alternating fibre orientation of adjacent lamellae.**

Testing began with three preconditioning cycles of 10% tensile strain at a rate of 1%/s.

Following preconditioning, samples were tensioned to 50% strain at 1%/s. Force and

displacement data were sampled at 100 Hz by the Labjoy software (Ustretch, Cellscale, Waterloo, ON).

### 3.3.3. Lamellar Adhesion Test

Following the excision of the OAF for the tensile test described in section 3.2.3, FSUs were transected to allow extraction of multilayered posterolateral AF specimens proximal to the site of EP fracture. Adjacent lamellae of multilayer specimens were separated with a scalpel to create two tabs of adequate size (Figure 9) to be gripped by the screw-driven clamps attached to the UStretch (Cellscale) system.

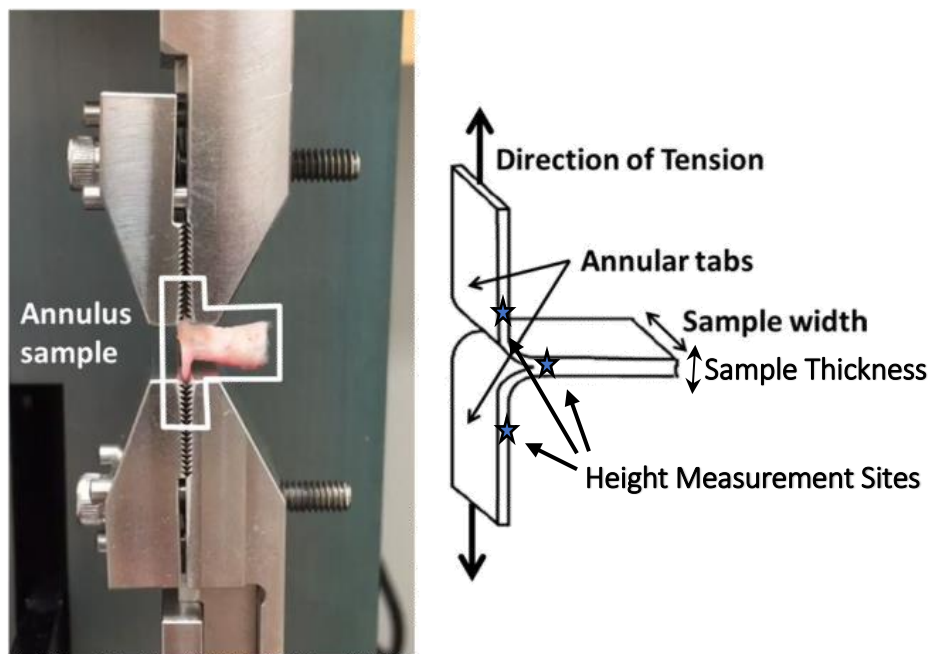


**Figure 9. Specimen mounted in UStretch machine (Cellscale, Waterloo, ON) prior to 180° peel test (left). Illustration of annular tabs created in specimens. Stars indicate the location where specimen height was measured. Image obtained from Gregory, Bae, Sah and Masuda (2012).**

## ENDPLATE FRACTURE

A laser displacement sensor (IL-065, Keyence, Mississauga, ON) was used to measure the height of specimens at three sites. The width of each annular tab, along with the width of the juncture where the tabs connect, were measured, and the mean of these three measurements was selected to represent sample width. Once mounted, the sample was subjected to a 180° peel test which acted to separate the annular tabs in opposite directions at 0.5mm/s until complete detachment. Force and displacement data were collected during the peel test by Ustretch (Cellscale) software, sampled at 100 Hz.

### **3.4. Data Analysis**

#### **3.4.1. Compression-to-Failure Analysis**

Force and displacement data were recorded during the compression-to-failure protocol. These measures were gathered using MTS Test Suite software, and sampled at 100Hz. A number of variables of interest were obtained from the force-displacement relationship (Figure 10): (1) Ultimate strength: the greatest magnitude of force achieved during the test prior to specimen failure. (2) Stiffness: the slope of the linear portion of the force-displacement curve. (3) Displacement at failure: the extent to which the tissue deformed at the point of failure.

Ultimate strength is of interest because damage to the EP is believed to be highly correlated with the development of DDD (Dudli, Haschtmann, & Ferguson, 2012). Therefore, EP fracture was identified visually, denoted by termination of the linear region of the force-displacement curve, in accordance with the protocols employed by Renau et al. (2004). Force was normalized to specimen EP cross-sectional area and presented in megapascals (MPa).

Displacement at failure was calculated by subtracting the height of specimens at their ultimate strength from their original pre-compression height. Due to losses in IVD height and dehydration of the NP correlating so highly with LBP and spinal dysfunction (Cassinelli & Kang, 2000), this was the final variable of interest for the compression-to-failure protocol.

## ENDPLATE FRACTURE

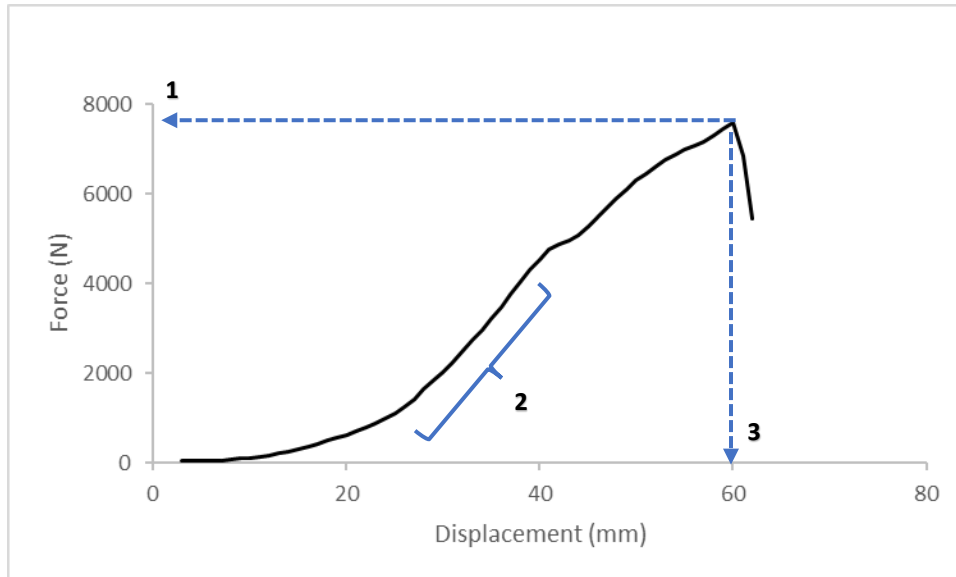


**Figure 10. Force-displacement curve from specimen #31 (fractured at 15mm/s) illustrating the variables of interest for the compression-to-failure analysis. Variables are as follows: (1) ultimate strength, (2) stiffness, and (3) displacement at failure.**

### 3.4.2. Tensile Strength Analysis – Bilayer AF samples

Tissue stress was calculated by dividing tissue force by specimen cross-sectional area.

Measurements of specimen height (via laser displacement sensor) and width (via ImageJ software) were used to calculate the cross-sectional area for each tissue sample. Stretch ratio was calculated by dividing the current rake-to-rake displacement by the original length plus one.

Tissue stress was reported at the following stretch ratios: 1.15 (15% strain) and 1.3 (30% strain).

In an experiment conducted by Snow et al. (2018), tensile stress of AF specimens was examined at a stretch ratio of 1.3, and in order to compare tensile tests, this strain value was selected for the present study. However, 7 of the 27 OAF specimens tested in this experiment failed to reach a strain ratio of 1.3 before either visible tearing of tissue, or slippage of tungsten rakes occurred to specimens. This inability to achieve a strain ratio of 1.3 prompted the additional comparison of specimens at a strain ratio of 1.15.

The stiffness of specimens was calculated by fitting a trendline to an  $R^2$  of  $>95.0\%$  of the linear region of specimens' stress-stretch ratio curve (Figure 11). The slope of the trendline represented specimen stiffness, and the end of the toe region was defined as the region where the stress-stretch ratio curve began its linear ascent (Figure 11). Stress and stretch ratio values were recorded at the end of the toe-region.

## ENDPLATE FRACTURE

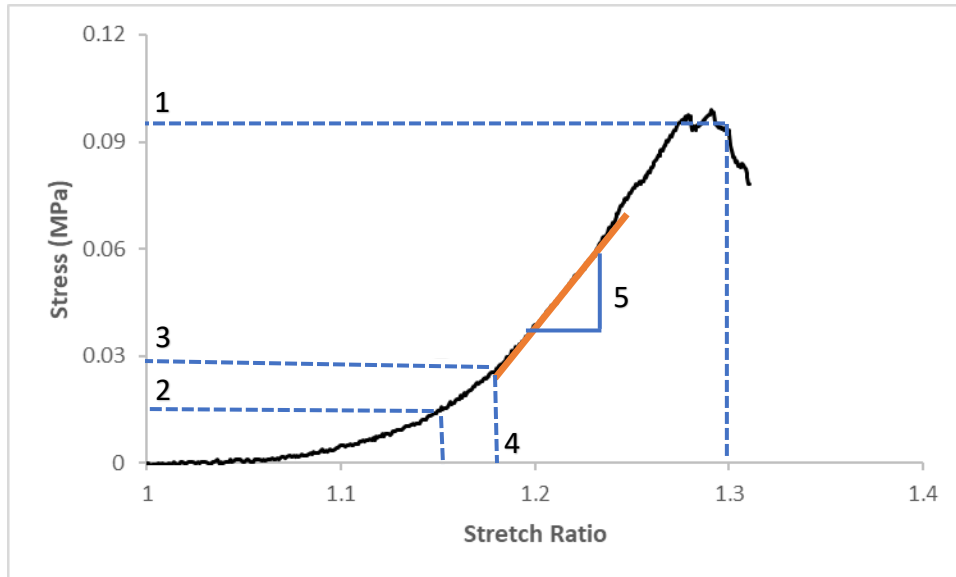


**Figure 11. Stress versus stretch ratio illustrating bilayer tensile test variables of interest for Specimen #20. Variables are as follows: (1) Stress at stretch ratio of 1.3, (2) Stress at strain ratio 1.15, (3) Stress at end of toe region (4) Strain ratio at end of toe region (5) Stiffness (orange line).**

### 3.4.3. Lamellar Adhesion Analysis – Peel test samples

Average peel strength was determined by calculating the average force over the plateau region of the test (indicating the region of delamination; Figure 12) and then dividing this value by the average bond width of the tissue sample. Peel strength was measured in N/mm. Additionally, peel strength variability across the plateau region was analyzed by calculating the standard deviation of force values across the selected plateau.

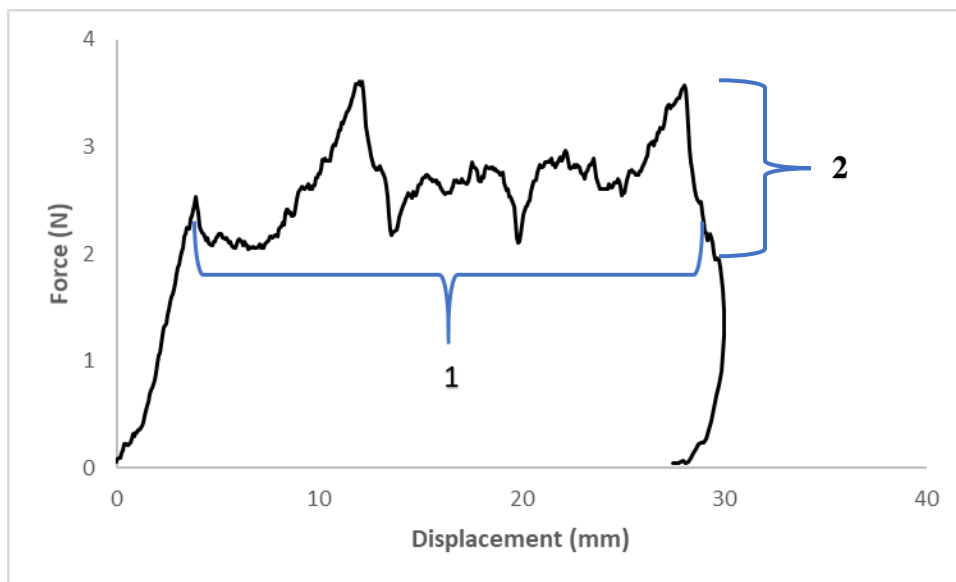


**Figure 12. Lamellar adhesion test of Specimen #27 illustrating plateau region where peel strength (1) and peel strength variability (2) were quantified.**

### 3.5. Histological Procedure

Histological examination was conducted on posterolateral segments of AF harvested from 8 different FSUs. Two FSUs were selected for use in each condition: fast (15mm/s), medium (1.5mm/s), and slow (0.15mm/s), with an additional two remaining unfractured and receiving preconditioning only, to serve as controls. Following loading, the posterior elements of FSUs were removed, granting access to the posterior AF. AF specimens were transversally sectioned out of FSUs taking care to remove the AF from as close to the cartilage of the EPs as possible. Specimens were placed in 10% formalin (Fisher Scientific) for a minimum of 48 hours before being sent to the Ontario Veterinary College (Guelph, Ontario) for paraffin embedding and hematoxylin and eosin (H&E) staining. H&E stained slides were assessed using an Axiolab microscope (Zeiss).

Harvey-Burgess and Gregory (2019) found that following a static compression and twist protocol, twisted bovine caudal IVDs demonstrated deficient mechanical properties compared to their untwisted counterparts. Furthermore, this weakening of twisted tissues seemed to coincide with increased visible damage during histological analysis. Harvey-Burgess and Gregory (2019) identified intralamellar clefts in their AFs, predominantly at the juncture of the IAF-OAF. Figure 13 shows sample images from the study conducted by Harvey-Burgess and Gregory (2019), illustrating some of these damage patterns.

## ENDPLATE FRACTURE

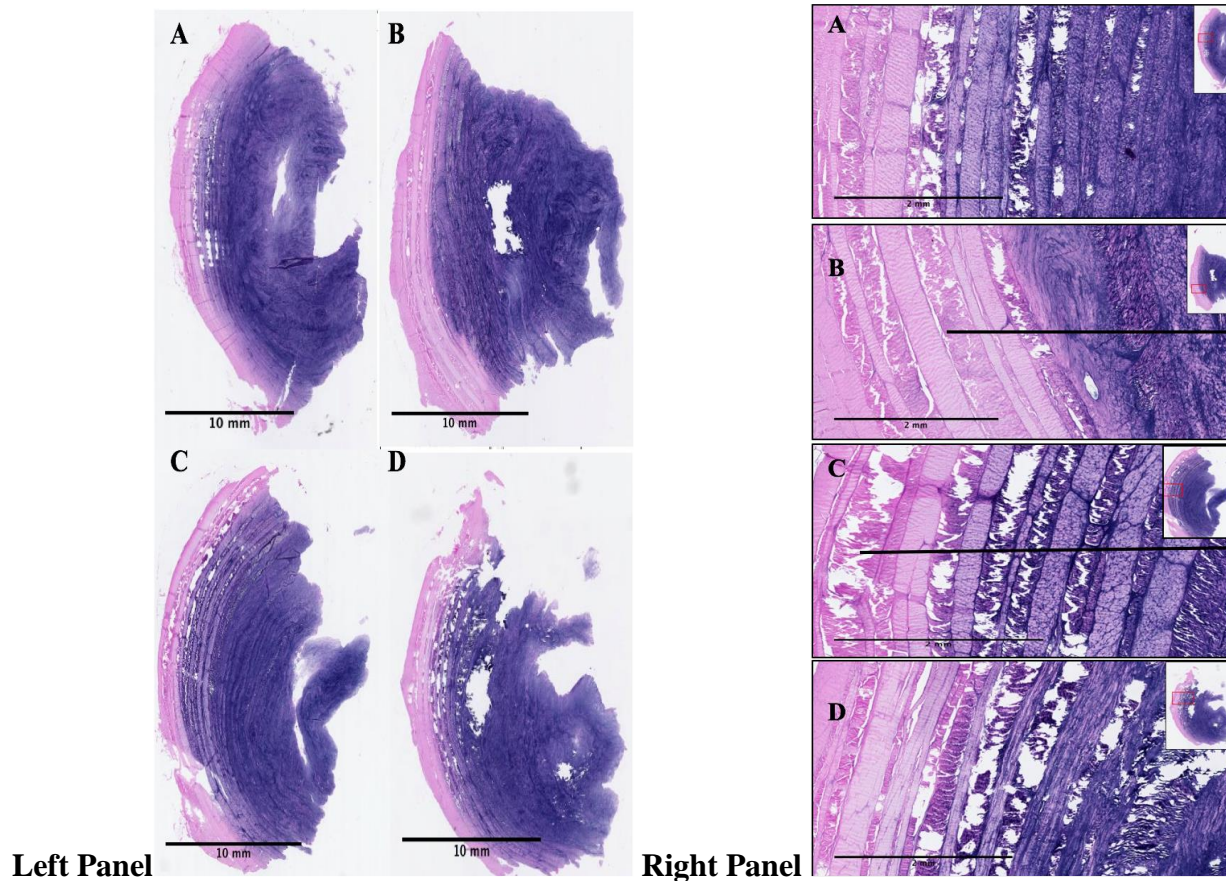


**Figure 13. Histological segments of AF, H&E stained following 2 hour twist and/or axial loading protocol. Axial loading was applied statically at 1000N, twist was held statically at 12°. Images in the right panel demonstrate magnified view of damage patterns observed in the mid-AF region of specimens in the left panel. A) Images of control specimen that received neither twist nor compression. B) Images of specimen that received only compression. C) Images of specimen that received only twist. D) Images of specimen that received combination compression/twist. Increased visual disruption was observed in twist conditions, with the combination twist/compression demonstrating the greatest amount of damage. Images obtained from Harvey-Burgess and Gregory (2019).**

### 3.6. Statistical Analysis

A mixed-factor analysis of variance (ANOVA) was applied to the variables of interest expressed in Table 1. The mixed-factor ANOVA treated spinal level (C3/4 versus C5/6) and rate of compression (15mm/s; 1.5mm/s; 0.15mm/s) as fixed effects, while the animal from which FSU specimens originated was treated as a random effect due to the minor, but unavoidable variation when experimenting on biological tissues. Significant observations were analyzed via Tukey-Kramer post-hoc comparisons with respect to the effects of spinal level and rate of compression. The level of significance for statistical analyses was set at 0.05.

**Table 1. Variables of Interest for Compression-to-failure, Tensile test, and Lamellar adhesion test.**

<b>Compression-to-Failure</b>	<b>Bilayer Tensile Test</b>	<b>Lamellar Adhesion Test</b>
Ultimate strength (N/mm <sup>2</sup> )	Stress at strain ratio 1.3 (MPa)	Peel strength (N/mm)
Displacement at Failure (mm)	Stress at strain ratio 1.15 (MPa)	Peel Strength variability (N/mm)
Stiffness (MPa)	Stiffness (MPa)	
	Stress end of toe region (MPa)	
	Strain ratio end of toe region	

## **4. Results**

### **4.1. Endplate Fracture Morphology**

In the present experiment, all of the specimens sustained an EP fracture, and fracture was identified during FSU compression by an audible ‘pop,’ along with visualization of a rapid downward inflection in the force tracing on the force-displacement curve (Figure 10). Fracture always occurred in the cranial EP often with further propagation vertically downward through the inferior vertebrae of the FSU (Figure 14). Fracture patterns ranged from small, non-displaced fractures, visible only with removal of the NP (Figure 14, b), to step-fractures with gross displacement of the posterior epiphyseal plate (Figure 14, d). Damage propagation down into the vertebral bodies occurred more regularly in the vertical than transverse direction (Figure 14, e and f), although neither pattern was infrequently observed. Anecdotally, the more damaged the EP, the more externally-visible fractures were in vertebral bodies.

An additional detail of interest was that, due to 0.15mm/s being such a slow rate of compression, multiple fracture-like fluctuations occurred to the force values in the force-displacement curve during many of the compression-to-failure trials, making identification of the moment of collapse difficult. More likely structural collapse of vertebrae occurred in stages, and the buckling of trabeculae and the small irregularities noted as inflections on the force-displacement curve may have marked internal events leading up the final, observable failure of the EP (Figure 15).

## ENDPLATE FRACTURE

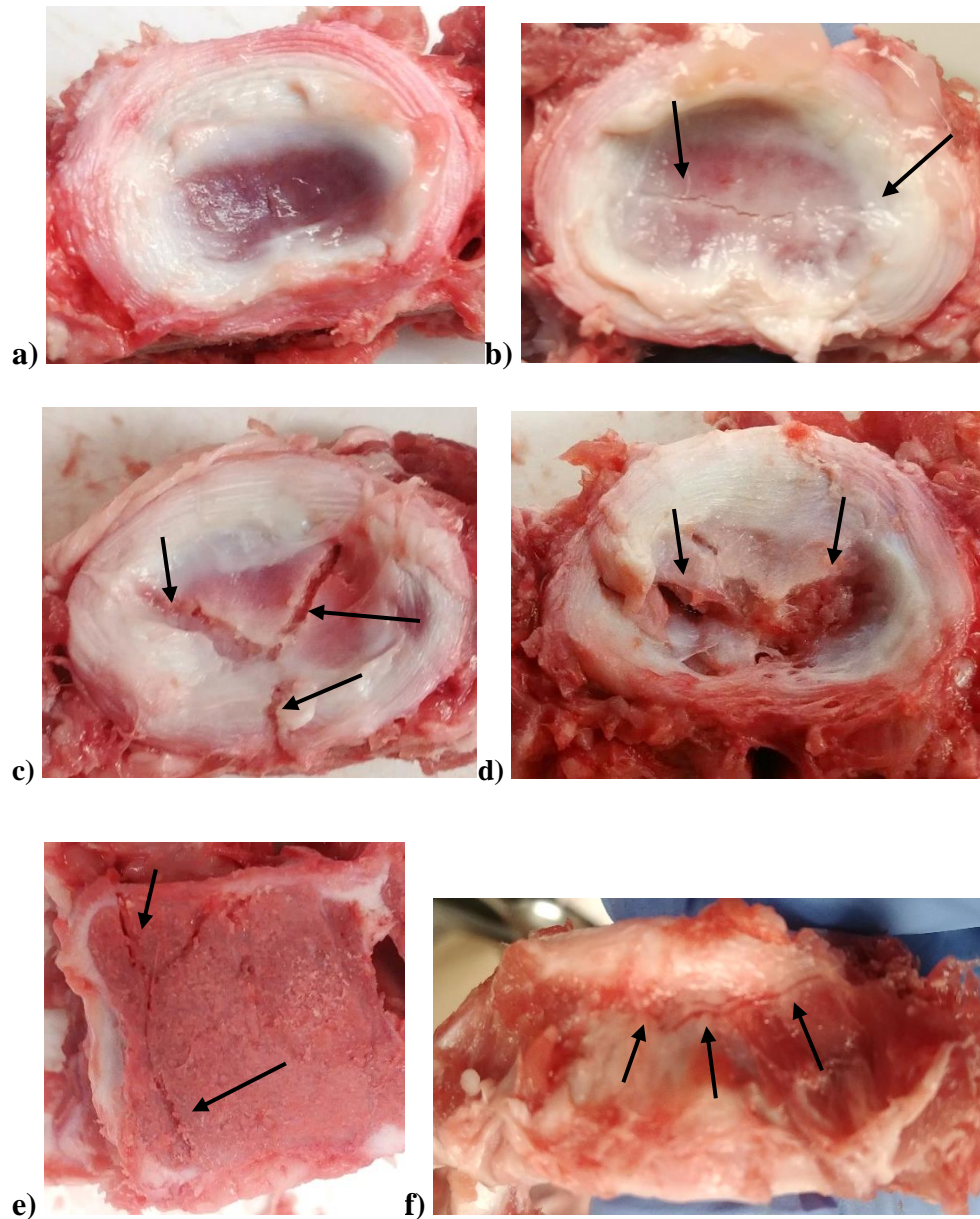


**Figure 14: a) EP of unfractured, control C3/4 level. b) Transverse fracture across EP, C3/4. c) Stellate fracture pattern of C3/4 EP. d) Step-fracture of C5/6 vertebra with inferior translation of vertebral body. e) C5/6 level vertebra transected in frontal plane to expose internal fracture propagation. f) Externally-visible transverse vertebral fracture of C4 vertebra (arrow).**

## ENDPLATE FRACTURE

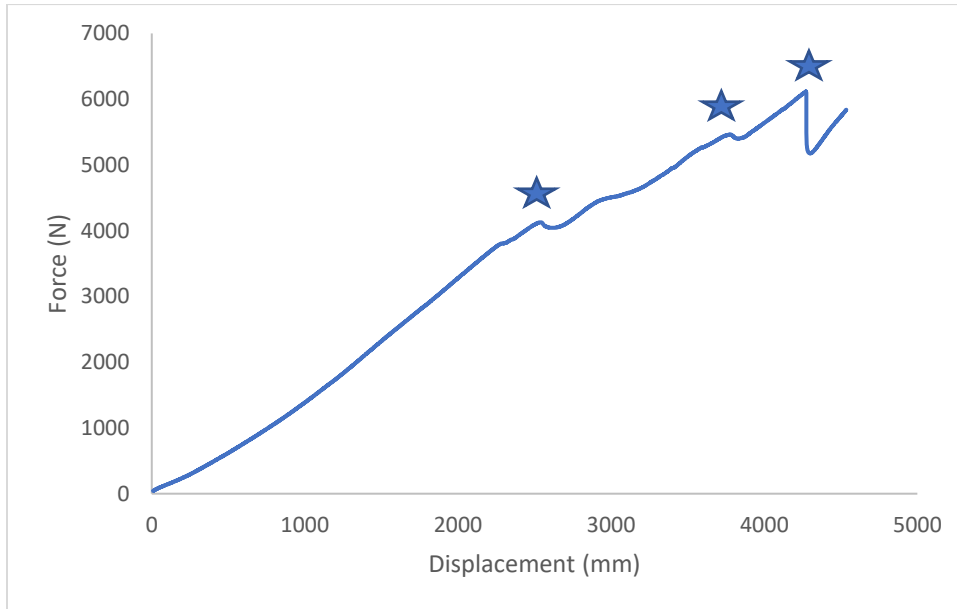


**Figure 15. Force-displacement data illustrating sub-fracture events (1 and 2) observed during slow-compression trial of specimen #18, prior to final EP fracture (3).**

## 4.2. Compression-to-Failure Results

Rate of compression was demonstrated to significantly affect FSU ultimate strength ( $p=0.0197$ ), and Tukey-Kramer post hoc analysis indicated that fast and medium speeds did not differ ( $p=0.7969$ ); however, fast and medium speeds resulted in 11.45% ( $p=0.0236$ ) and 17.54% ( $p=0.0126$ ) greater ultimate strength compared to the slow rate, respectively. The mean ultimate strength for fast, medium, and slow-compression FSUs were 10.83N/mm (SE 0.84), 11.63N/mm (SE 0.48), and 9.59N/mm (SE 0.65); Figure 16 and Table 2.

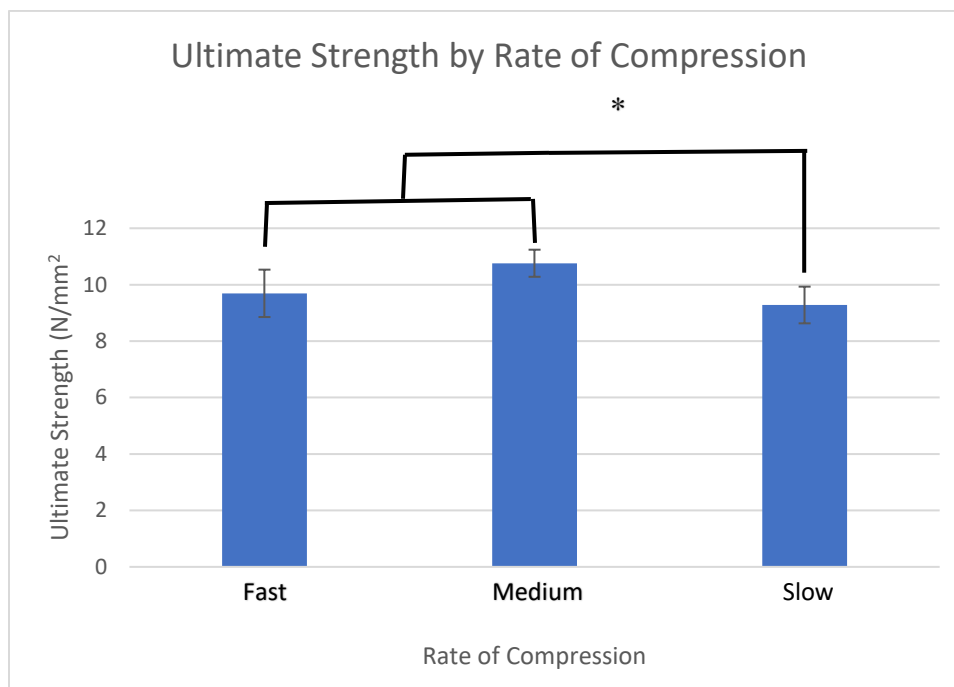


**Figure 16. Results for ultimate strength by rate of compression fast (15mm/s), medium (1.5mm/s), and slow (0.15mm/s). Star denotes significance (fast and medium were both significantly different to slow, but not from one another).**

## ENDPLATE FRACTURE

The fast-compression condition exhibited significantly more FSU stiffness compared to the medium ( $p= 0.0259$ ) and slow ( $p= 0.0293$ ) compressions (Figure 15). Compression-to-failure at 15mm/s resulted in a mean stiffness of 1518.91MPa (SE 178.19) which was 19.41% higher than the 1224.1MPa mean for the medium condition (SE 226.38), and 31.93% greater than the ultimate strength of 1151.31MPa for slow-fracture specimens (SE 119.77). Comparatively, there was no difference in the stiffness of tissues compressed at the medium versus slow velocities ( $p= 0.7472$ ).

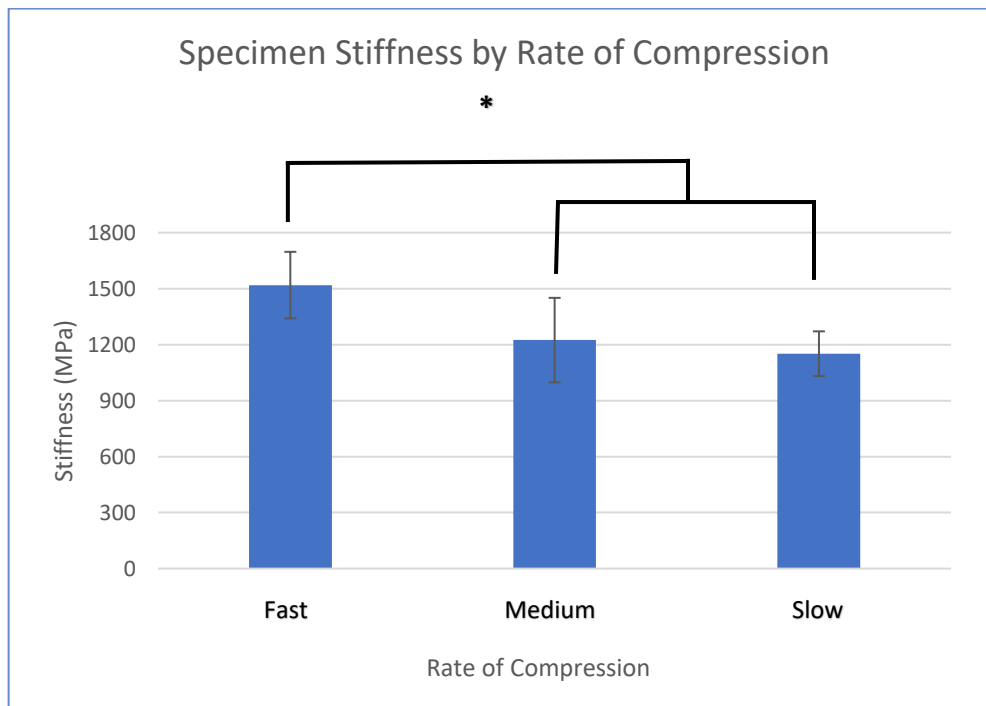


**Figure 17. Comparison of mean FSU stiffness in fast (15mm/s), medium (1.5mm/s), and slow (0.15mm/s) compression. Star denotes significance (fast was significantly different to medium and slow, medium and slow conditions were not different from one another).**

## ENDPLATE FRACTURE

Specimens extracted from the C3/4 spinal level had a mean stiffness of 1466.3MPa (SE 162.2) as compared to 1108.91MPa for C5/6 specimens (SE 106.55), demonstrating 32.23% greater stiffness in C3/4 FSUs during compression-to-failure ( $p= 0.0255$ ).

The mean displacement of fast, medium, and slow-rate specimens was 7.51mm (SE 0.72), 8.06mm (SE 0.64), and 8.09mm (SE 1.44) respectively, and these were not found to be significantly different (see Table 2).

**Table 2. Compression-to-Failure results for fixed effects of spinal level (C3/4 versus C5/6), rate of compression (15mm/s, 1.5mm/s, 0.15mm/s), and their interaction effects. Results found to be significant are underlined. N=10.**

	<b>Rate of Compression</b>	<b>Spinal Level</b>	<b>Interaction of Rate of Compression with Spinal Level</b>
<b>Ultimate Strength (N/mm)</b>	<b><u>P= 0.0197</u></b>	<b>P= 0.0913</b>	<b>P= 0.4788</b>
<b>Stiffness (MPa)</b>	<b><u>P= 0.0466</u></b>	<b><u>P= 0.0255</u></b>	<b>P= 0.2528</b>
<b>Displacement at Failure (mm)</b>	<b>P= 0.6986</b>	<b>P= 0.0869</b>	<b>P= 0.1658</b>

### 4.3. Bilayer Tensile Test Results

The rate compression to failure did not significantly alter the mechanical properties of the AF with regards to any of the variables of interest quantified in the bilayer tensile test. Bilayer tensile test results are summarized in Table 3. The mean stress tissues experienced at strain ratios of 1.3 were 0.11MPa (SE 0.04), 0.14MPa (SE 0.03), and 0.14MPa (SE 0.05) for bilayer samples extracted from FSUs compressed at the fast, medium, and slow rates of fracture, respectively. Mean stress experienced by tissues at strain ratios of 1.15 were 0.04MPa (SE 0.02), 0.02MPa (SE 0.01), and 0.03MPa (SE 0.01) for fast, medium, and slow, respectively. The mean stiffness values recorded for bilayer samples from the fast, medium, and slow compression FSUs were 0.91MPa (SE 0.32), 1.11MPa (SE 0.17), and 1.33MPa (SE 0.44). With regards to the toe regions identified during testing, the mean stress observed in specimens extracted from fast (15mm/s), medium (1.5mm/s), and slow-compressed (0.15mm/s) FSUs were 0.07MPa (SE 0.01), 0.05MPa (SE 0.02), and 0.05MPa (SE 0.02), and these values occurred at strain ratios of 1.18 (SE 0.02), 1.22 (SE 0.02), and 1.21 (SE 0.03), respectively.

## ENDPLATE FRACTURE

**Table 3. Bilayer Tensile Test Results for fixed effects of spinal level (C3/4 versus C5/6), rate of compression (15mm/s, 1.5mm/s, 0.15mm/s), and their interaction effects.**

	<b>Rate of Compression</b>	<b>Spinal Level</b>	<b>Interaction of Rate of Compression with Spinal Level</b>
<b>Stress at Strain Ratio 1.3 (MPa)</b>	<b>P= 0.7730</b>	<b>P= 0.4718</b>	<b>P= 0.5346</b>
<b>Stress at strain ratio 1.15 (MPa)</b>	<b>P= 0.6777</b>	<b>P= 0.7899</b>	<b>P= 0.5962</b>
<b>Stiffness (MPa)</b>	<b>P= 0.7335</b>	<b>P= 0.7841</b>	<b>P= 0.9588</b>
<b>Stress End of Toe Region (MPa)</b>	<b>P= 0.8682</b>	<b>P= 0.9895</b>	<b>P= 0.5018</b>
<b>Strain Ratio End of Toe Region</b>	<b>P= 0.4013</b>	<b>P= 0.1106</b>	<b>P= 0.8748</b>

#### 4.4. Lamellar Adhesion Test Results

The mean lamellar adhesion strength recorded among the slow, medium, and fast-fracture groups were 3.6N/mm (SE 0.88), 3.18N/mm (SE 0.53), and 2.89N/mm (SE 0.62) ( $p=0.5419$ ), and their peel strength variabilities were 1.24N/mm (SE 0.79), 0.47N/mm (SE 0.08), and 0.41N/mm (SE 0.1) ( $p=0.4014$ ), respectively. Results for the effect of rate of compression, spinal level, and their interactions are illustrated in Table 4; no significant effect of rate of compression, spinal level, or their interaction was observed.

**Table 4. Lamellar Adhesion Test Results for fixed effects of spinal level (C3/4 versus C5/6), rate of compression (15mm/s, 1.5mm/s, 0.15mm/s), and their interaction effects.**

	<b>Rate of Compression</b>	<b>Spinal Level</b>	<b>Interaction of Rate of Compression with Spinal Level</b>
<b>Peel Strength (N/mm)</b>	<b>P= 0.5419</b>	<b>P= 0.5060</b>	<b>P= 0.1812</b>
<b>Peel Strength Variability (N/mm)</b>	<b>P= 0.4014</b>	<b>P= 0.2588</b>	<b>P= 0.3348</b>

The study conducted by Snow et al., (2018) served as the basis for much of the present research question. Therefore, in order to strengthen comparisons between the present study and the results

## ENDPLATE FRACTURE

obtained by Snow et al. (2018), 4 additional FSUs (2 from level C3/4, and 2 from level C5/6) were extracted, preloaded, and then subjected to lamellar adhesion testing (according to procedure in section 3.3.) without any further mechanical influence. Mean peel strength among these controls was 3.76N/mm (SE 0.29).

#### **4.5. Histological Results**

Histological examination did not detect any discernible patterns of damage attributable to annular delamination of specimens. Section 3.5. outlines patterns of annular damage as observed in bovine annular specimens, and these patterns of damage were not visualized in specimens in the present experiment (Figure 17). Due to the similarity in the regular, uninterrupted orientations of lamellae within specimens, no discernible differences in damage can be reported between the fast, medium, slow, and control conditions.

## ENDPLATE FRACTURE

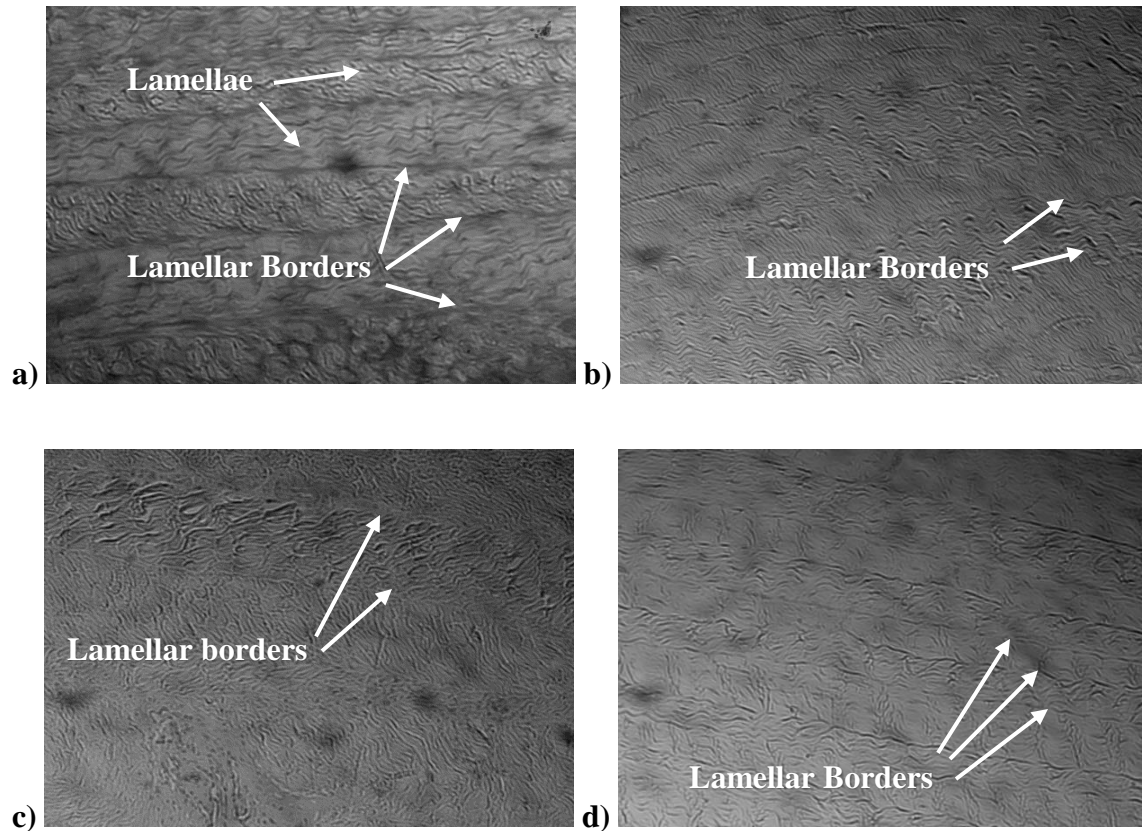


**Figure 18. H&E staining (10X magnification) of the posterior AF obtained from the IVD of a fast-rate loaded (a), medium-rate loaded (b), slow-rate loaded (c), and control (d) FSU. For a-c, each FSU sustained an EP fracture. For the control (d) FSU, the specimen was only preloaded for 15 minutes and did not sustain a fracture. In each pane, lamellae and lamellar borders are identified. In all conditions, no notable delamination between lamellae was observed. In all four pictures the bottom is most proximal to the NP in the radial direction and the top of the pictures is most distal from the NP and nearest the OAF region.**

## 5. Discussion

The present experiment illustrated that the point at which EPs fractured during compressive loading was significantly impacted by both the rate at which FSUs were loaded, and the spinal level from which specimens were extracted, but that these differences did not translate to changes in the mechanical properties of the AF or changes in the appearance of the lamellae histologically.

The fastest velocity of compression produced the stiffest response in IVDs, fulfilling one of the pre-experiment hypotheses. Additionally, while FSUs compressed at the fastest velocity did not demonstrate the greatest ultimate strength as predicted, the similarity in ultimate strength and stiffness expressed between tissues loaded at 15mm/s and 1.5mm/s suggests that these velocities may have elicited a similar biomechanical response which was different from FSUs compressed at the slowest rate. Both experimental and finite element modelling has concluded that the viscoelastic response of the NP is influenced by the amplitude and velocity of applied forces (Farrell & Riches; and Rao & Dumas, 1991). Increased compression velocities are purported to incite a more solid response from the NP where it becomes stiffer and less deformable (Farrell & Riches, 2012). Likely, the similar ultimate strengths and stiffnesses observed in specimens compressed at 15mm/s and 1.5mm/s stemmed from these compression velocities inciting a similar amount of viscous stiffening of the hydrated NP, whereas slow compressions occurred at velocities commensurate with a less solid, and more fluid-like response. In the present experiment, fast and medium-compression conditions likely elicited a similar response in the NP with regards to the viscous 'stiffening' that occurs with resistance of compression. Conversely,

## ENDPLATE FRACTURE

compressions at the slowest rate (0.15mm/s) may have permitted the greatest amount of displacement in FSUs (as was hypothesized before the experiment, though this trend did not prove significant), by incurring the least amount of NP ‘stiffening’ during compression.

While significant differences in ultimate strength and stiffness were observed across rate of compression and spinal level, no significant differences were detected in the mechanical properties of AF specimens, opposite to this study’s initial hypothesis. The lack of observed significance in the present experiment was likely due to the use of compressive force rates below what would be necessary to negatively impact the AF. FSU stiffness values permitted estimates of the rates of internal pressurization incurred by FSUs, and compressions of 0.15mm/s, 1.5mm/s, and 15mm/s were predicted to result in a maximum internal pressurization of 0.45MPa/s. Conversely, Snow et al. (2018) detected a 31% reduction in peel strength after internally pressurizing FSUs at a mean velocity of 17.5MPa/s with their manual hydraulic system. The maximum compression velocity used in this experiment, while impactful on the ultimate strength and stiffness of specimens, appeared much too slow to initiate the internal-pressurization mechanism posited to be responsible for the reduced peel strength observed by Snow et al. (2018). Figure 19 compares the peel strengths of specimens from the present experiment to fractured and unfractured controls from the study conducted by Snow et al. (2018). Interestingly, the peel strength of the unfractured, untested controls (2.91N/mm) reported by Snow et al. (2018) is only 9.63% less than the combined mean peel strength of the fast, medium, and slow-compressed FSUs from the present experiment (3.22N/mm, SE 0.39).

## ENDPLATE FRACTURE

Additionally, the fractured specimens in this experiment displayed 37.58% greater peel strength than the EP-fractured specimens of Snow et al. (2018). To strengthen comparisons between Snow et al.'s (2018) results and those of the present experiment, four additional control FSUs were examined. Mean peel strength among these controls was 3.76N/mm (SE 0.29), proving to be only 4.44% greater than the present experiment's fast-compressed FSUs; the closest in rate to the fracture specimens by Snow et al (2018); albeit still much slower, suggesting that it is likely the manner in which specimens fracture (rapid loading) rather than the actual occurrence of an EP fracture, that affects AF adhesion strength. As a result, such evidence would infer that EP fracture itself is not a pivotal aetiological event in the development of DDD, but rather, that disruptions of the IVD at the junction of interlamellar matrices may be the critical factor in DDD's onset.

## ENDPLATE FRACTURE

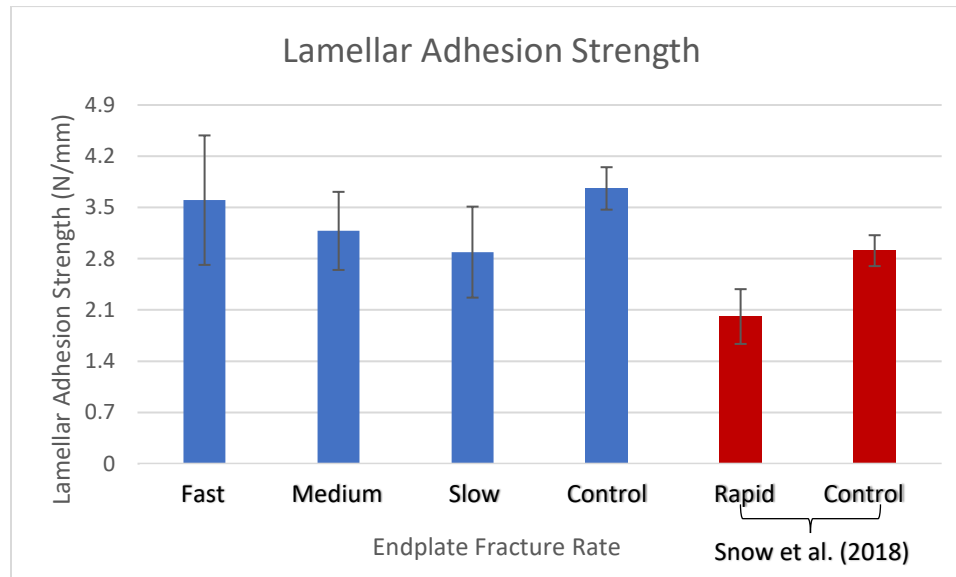


**Figure 19. Mean peel strengths by rate with additional controls performed for comparison, as well as the rapidly-fractured (Rapid, red column), and untested controls (Control, red column) from the experiment by Snow et al. (2018).**

Histological analysis of AF specimens supports the non-significant differences reported between the mechanical properties of the three experimental groups. The development of clefts or small pockets of space between lamellae signifies a disturbance in the adhesion between adjacent layers. Such irregularities can develop within single layers in the form of intralamellar delamination, but delamination is more commonly reported as a loss of adhesion between adjacent layers (interlamellar delamination) than direct fibrous rupture. During compression, the tendency for the NP to migrate toward lower-pressure areas of the IVD is thought to be responsible for this mechanism of cleft-formation during delamination (Adams et al., 2013). Gross dissections conducted by Snow et al. (2018) identified small pockets of hydraulic fluid in the nuclear cavity and in between adjacent lamellar layers. In the present experiment, lamellar

## ENDPLATE FRACTURE

borders and AF fiber organization within specimens did not appear to be affected by loading rate; the expected patterns of injury and disruption from the loading mechanism described by Snow et al. (2018) appeared entirely absent. This lack of visual damage corroborates the present study's findings that the forces incurred by the three different rates of compressive velocity were insufficient to cause adequate internal-pressurization of FSUs, such that AF tissue could be damaged prior to EP failure. This lack of visual disruption qualitatively verifies the non-significant differences in the mechanical properties of specimens.

Presently, research demonstrates that pain and radiological findings do not necessarily correlate with LBP (Costi, Freeman, & Elliott, 2011). As such, it is of great concern as to how DDD and LBP might be predicted or diagnosed at earlier stages so that continued, unmitigated pathological advancement of the condition does not go undiagnosed. The present experiment demonstrated that the EP is consistently the site of failure in compressed FSUs, which may suggest the need for clinical re-evaluation of EP-fracture diagnostics, rehabilitation programs, and prognoses for patients who have undergone such an injury. However, the animal model and mechanism of loading utilized in the present experiment limit the assertions that can be made regarding human injuries. Gymnastics, snowboarding and skiing, mountain-biking, and numerous other human activities expose individuals to possible falls and high-velocity landings that may be capable of injuring the AF in combination with EP injury. However, injury in these sports typically occurs with complex, multi-plane movements, and not necessarily in the young, healthy spines modeled by the porcine cervical region. As such, future research should seek to describe modes of injury to the EP throughout a greater range of velocity, and in combination-loading scenarios. Such improvements, paired with animal models of varying physiological compositions (for example,

chondrodystrophic canines), might broaden the inferences that can be made regarding EP injuries in the human condition, and better inform clinical policy and practice.

However, the prevalence of high-velocity human activities highlights the importance of the mechanism by which Snow et al. (2018) identified a reduction in peel strength following rapid internal pressurization of an IVD; spotlighting the need to examine this potential factor.

Evidence in the present experiment, in conjunction with results from Snow et al. (2018) suggest that mere presence of an EP fracture may be insufficient to reduce the adhesion strength of lamellae, but rather the mechanism by which EP fracture occurs and how the AF is stressed may be the more important factor in AF dysfunction. Section 1.2.2. outlined two possible mechanisms that may initiate delamination of the AF, however, it is currently not known whether rapid internal pressurization of an IVD without EP fracture could still reduce the peel strength of specimens' AFs. A study conducted by Gregory et al. (2009) sought to examine the rate-sensitivity of bilayer annular specimens strained at speeds of 1%/s, 2%/s, and 4%/s. Their work concluded that the mechanical properties of the AF were rate-independent below strain rates of 4%/s, and this coincides well with the rate-independence reported of collagenous tendons and ligaments at slower velocities of strain (Chambers, Herod, & Veres, 2018; Clemmer, Liao, Davis, Horstemeyer & Williams, 2010; Jung, Fisher, & Woo, 2009; Weiss, Gardiner, & Bonifasi-Lista, 2002). Both IVD research and tendon and ligament studies lead the present thesis to posit that compression leading to EP fracture at velocities of 15mm/s or less do not have a significantly different impact on the mechanical properties of the AF. However, the work conducted by Snow et al. (2018) illustrates how the conditions for EP fracture at high velocity may also predispose the AF to delamination. Whether or not EP fracture is necessary at high-

## ENDPLATE FRACTURE

velocity for annular weakening remains a pertinent question in the field of spinal research, as the clinical picture regarding EP injury and AF dysfunction remains incomplete.

Interestingly, the present experiment also demonstrated a significant difference in the ultimate strength of C3/4 versus C5/6 spinal levels, along with significant differences in ultimate strength and stiffness of FSUs in response to loading rate. The 32.23% greater stiffness observed in C3/4 FSUs compared to C5/6 FSUs is likely a product of their more neutral posture in the porcine cervical spine. In humans, the majority of lordosis in the lumbar spine occurs in the L4 and L5 vertebrae, and the drastic extension of these ‘transitional’ segments seems to result in increased rates of degeneration (Hadjipavlou, Tzermiadianos, Bogduk, & Zindrick, 2008). As such, it is hypothesized that the extended posture of C5/6 segments resulted in a mechanically-disadvantageous position as compared to the more neutrally-positioned C3/4 segments, and is therefore responsible for the differences observed across spinal levels. As expressed in section 1.1.4., young, immature mammalian spines fail in compression along their posterior epiphyseal plate. The lordotic posture of human lumbar and porcine cervical spines seems to concentrate stress distributions in the posterolateral aspects of the IVD. In the present experiment, the greater lordosis of C5/6 compared to C3/4 specimens was posited to account for their decreased ultimate strength, and morphological observations compliment such an hypothesis, because C5/6 specimens expressed more posteriorly-oriented fractures in their EPs (Figure 14., d and e), whereas damage to C3/4 levels tended to be more centrally-located (Figure 14., b and c).

### 5.1. Revisiting Objectives:

Section 2.1. outlines the three main objectives of the present experiment. Objectives were developed in order to better inform this study's hypotheses, and to outline the expected characteristics of IVDs in response to the selected rates of velocity.

- 1) The first objective of the present experiment was to elicit different magnitudes of viscoelastic responses from FSUs compressed at different velocities. The purpose was to elicit viscoelastic responses whose effects on AF tissue were different enough to be quantified mechanically.

The three rates of compression likely initiated different viscoelastic responses from FSUs, as seen in the significant differences between FSU stiffnesses and ultimate strengths (section 4.2.). However, some FSU compression characteristics appeared similar between the fast and medium-compressed FSUs, and the medium and slow-compressed FSUs. This suggests that greater differences in velocity be applied to groups to better illustrate differences in IVD behaviour across a range of viscoelastic responses.

- 2) The second objective was to accomplish EP fracture in all of the FSUs that were compressed to failure.

All FSUs compressed-to-failure, regardless of velocity, demonstrated failure of their cranial EPs. Consistent failure of the EP demonstrated the EP as the kinetic 'weak link' of the porcine cervical spine when compressed in the neutral posture. Failure patterns were consistent with pre-experiment hypotheses (section 2.2.).

- 3) The third objective was to quantify, visually examine, and then compare the effect that different FSU compression velocities had on specimens' AF tissue.

In combination, visual and mechanical data from the present experiment suggest that the velocities selected for FSU compression-to-failure were not different enough to demonstrate rate-sensitive alterations to AF tissue.

## 5.2. Revisiting Hypotheses:

Section 2.2. outlines hypotheses for the present experiment as they relate to the variables of interest for each of the three mechanical tests conducted. At the FSU level, the first pre-experiment hypothesis was:

- 1) Faster compression velocities were predicted to result in greater measures of ultimate strength, stiffness, and less displacement of FSUs prior to EP fracture, versus slower compression velocities.

There seemed to be a marked effect on the ultimate strength and stiffness of FSUs compressed at faster velocities. Stiffness was found to be greatest in fast-compressed FSUs fulfilling this pre-experiment hypothesis. Unexpectedly, medium-speed compressions elicited the largest ultimate strength from specimens, but the non-significant difference in mean ultimate strength between the medium and fast-compressed groups suggests that compressions of 1.5mm/s and 15mm/s may generate a similar viscoelastic response from tissues, partially-supporting this pre-experiment hypothesis. Unexpectedly, displacement was not found to be related to the point at which EPs fractured, and different velocities of compression did not result in different displacements to FSUs.

The second pre-experiment hypothesis related to whole-FSU compression was:

- 2) All FSUs, regardless of rate of compression, were predicted to sustain EP fracture.

Histological and morphological analyses revealed visible EP fracture(s) in all compressed FSUs, fulfilling this pre-experiment hypothesis.

## ENDPLATE FRACTURE

Analyses of posterior, bilayer OAF samples after EP fracture of FSUs was predicted to result in the following mechanical responses from specimens:

- 1) EP fracture sustained at the fastest compression rate was hypothesized to result in bilayer AF samples that would be more compliant, reach lower stress magnitudes, and displace to a greater degree than the slowest compression rate.

Counter to pre-experiment hypotheses, compliancy, degree of displacement, and the magnitudes of stress within tissues were unaffected by the rates of compression. No significant differences in tissue mechanics were detected at this level of analysis.

The final level of mechanical analysis was performed on multilayer samples, investigating their adhesion strength. This investigation was posited to result in the following observations:

- 1) Specimens compressed at the fastest velocity were predicted to display the lowest AF adhesion strengths and greatest adhesion strength variability compared to the slowest compression rate.

Counter to pre-experiment hypotheses, adhesion strength, and the variability of specimens' adhesion strengths were not impacted by the three rates of compression. Additional investigation reports non-significant differences in the adhesion strength of non-EP fractured controls compared to EP-fractured specimens. The lack of difference in adhesion strengths between the different fracture velocities and unfractured controls appears antithetical to the purported mechanism of injury associated with AF weakening post EP fracture. The present study advocates for future investigation of the relationship between EP fracture and AF weakening.

## 6. Limitations

Spinal research commonly incorporates animal models in place of human tissue due to the availability, cost-efficiency, and reduced ethical considerations that accompany their use. An additional benefit resides in the added information available to researchers regarding animals' diet and history of activity. However, animal models must be selected carefully, because although ample research attests to their merits in IVD research (Showalter et al., 2012; Beckstein, Sen, Schaer, Vresilovic, & Elliott, 2008; O'Connell, Vresilovic, & Elliott, 2007) there are still anatomical and compositional differences to be considered.

In relation to the present experiment, Beckstein, Sen, Schaer, Vresilovic, and Elliott (2008) demonstrated that when normalized by vertebra height and EP cross-sectional area, the compressive stiffness, and creep responses of porcine cervical FSUs are not significantly different than those of human lumbar FSUs. Anatomically, porcine cervical IVDs are limacon (Figure 20) in shape, possess posterior, articulating facets, have concaved EPs (Busscher, Ploegmakers, Verkerke & Veldhuizen, 2010) and compared to humans, have comparable ratios of proteoglycans in their NPs (Beckstein et al., 2008), and collagen contents in their NPs and OAFs (Showalter et al., 2012). However, Beckstein et al. (2008) reported less proteoglycan content in the IAFs of porcine cervical IVDs, and Showalter et al. (2012) demonstrated that porcine IVDs have more than double the collagen content than humans in their IAFs when normalized by dry weight. Morphological comparisons between human and porcine cervical IVDs are imperfect as well, because porcine cervical IVDs are significantly taller and narrower

than human IVDs (Busscher, Ploegmakers, Verkerke & Veldhuizen, 2010), lending them a greater range of motion in axial compression (Beckstein et al., 2008).

A final note regarding porcine cervical FSUs is that, owing to the difference between the weightbearing and non-weightbearing status of human lumbar versus porcine cervical FSUs, the mechanical disturbances responsible for long term remodelling or degeneration of the human spine cannot be said to be present in the porcine cervical spine. Pertaining to the present experiment, the differences in vertebral and IVD heights limit possible inferences from the present study in relation to the ranges of motion the human lumbar spine may undergo in similar loading scenarios. However, anatomical and functional similarities demonstrate that, in lieu of human tissue, the porcine cervical spine is the optimal model to represent the biomechanical responses of young, non-degenerated human lumbar spines in a compressive-loading scenario.

While the use of animal models in research curtails what can be definitively said about the human condition, their increased availability, population homogeneity, the knowledge available to researchers regarding diet, exercise, and health history, and the high levels of transferability present in a properly-selected model, permit inferences that can refine and improve research when it is applied to invaluable human specimens.

## ENDPLATE FRACTURE

## POSTERIOR

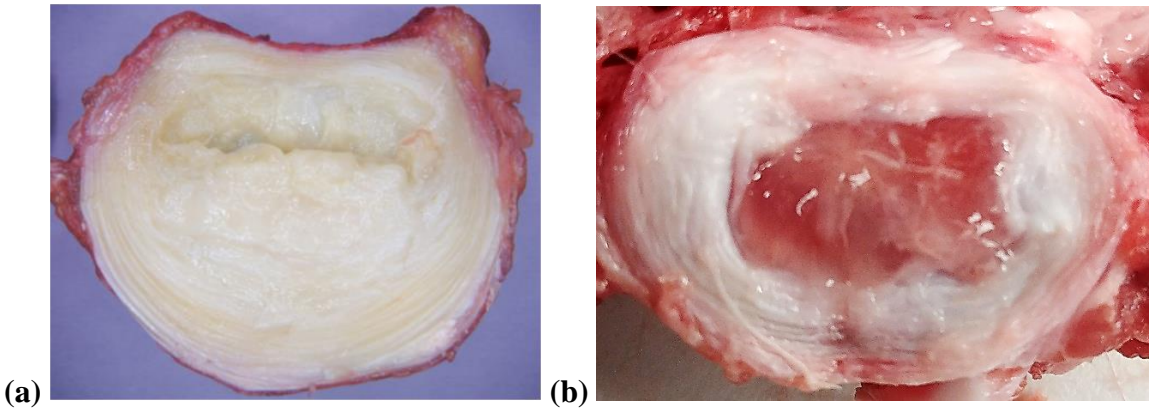


**Figure 20 (a) Human L4/5 lumbar IVD. (b) Porcine cervical 3/4 IVD.**

The lack of a defined break-detect in the compression algorithm in the present experiment necessitated qualitative identification of fracture. Fracture was denoted by an audible ‘pop’ and sharp inflection in force-displacement data. Upon observing these events, the compressive apparatus was immediately stopped and as a result, the degree of damage may have varied across samples. Difficulty in defining fracture-events is commonplace in fracture research, and technological advances present optimism in creating more precise future definitions.

Last, due to dissection techniques, the present experiment could only utilize bilayer samples from distal, posterior regions of the OAF, so tensile alterations to the IAF within IVDs cannot be commented on with the current data. Additionally, peel test configuration tended to target central layers of the posterior AF, so variations both regionally about the IVD, and proximally and distally within lamellar layers cannot be commented upon. However, the partitioning between lamellae becomes more obscure the more proximally located they are to the NP, so future studies will have to overcome this lack in distinct anatomical separation as well.

## 7. Conclusions

Results from the present study indicate that the mechanical responses of annular tissue are not significantly different following compressive EP fracture at velocities of 15mm/s and below. Additionally, the mechanism of annular buckling theorized to occur post EP-fracture failed to deform AF layers quickly enough, or far enough relative to one another that the elastic bonds of the interlamellar matrix were damaged. However, the observed stiffness and ultimate strength of specimens appeared to be significantly impacted by the velocity at which they were compressed, and these differences in whole-segment mechanics illustrate the need for future research to better understand the IVD's viscoelastic response to loading velocity.

In vivo, EP fracture seems to occur with rapid transmission of forces through an adolescent spine, such as the forces that might be incurred falling on one's backside. These conditions may or may not result in EP fracture, but the poorly defined link between EP fracture and annular weakening necessitates future examinations of whether adhesion strength reductions, such as those illustrated by Snow et al. (2018), can occur in a biologically representative EP fracture model. Such investigation would clarify the possible connection between EP fracture, high-velocity pressurization of the AF, and a predisposition to annular weakening later in life. A better understanding of possible interactions between high-velocity compressions and possible detriments to the spine may permit more accurate diagnoses from clinicians, and improve activity prescription for people at risk of incurring annular defects.

## 8. References

- Adams, M. A., Burton, K., Bogduk, N., & Dolan, P. (2012). *The biomechanics of back pain, 3<sup>rd</sup> Edition*. Elsevier health sciences.
- Adams, M. A., Freeman, B. J., Morrison, H. P., Nelson, I. W., & Dolan, P. (2000). Mechanical initiation of intervertebral disc degeneration. *Spine*, 25(13), 1625-1636.
- Adams, M. A., McNally, D. S., & Dolan, P. (1996). 'Stress' distributions inside intervertebral discs. *The Journal of Bone and Joint Surgery. British Volume*, 78-B(6), 965-972.
- Adams, M. A., Stefanakis, M., & Dolan, P. (2010). Healing of a painful intervertebral disc should not be confused with reversing disc degeneration: Implications for physical therapies for discogenic back pain. *Clinical Biomechanics*, 25(10), 961-971.
- Allan, D. G., Russell, G. G., Moreau, M. J., Raso, V. J., & Budney, D. (2005). Vertebral end-plate failure in porcine-and bovine models of spinal fracture instrumentation. *Journal of Orthopaedic Research*, 8(1), 154-156.
- Antoniou, J., Steffen, T., Nelson, F., Winterbottom, N., Hollander, A. P., Poole, R. A., Alini, M. (1996). The human lumbar intervertebral disc: Evidence for changes in the biosynthesis and denaturation of the extracellular matrix with growth, maturation, ageing, and degeneration. *Journal of Clinical Investigation*, 98(4), 996-1003.
- Aufdermaur, M. (1974). Spinal injuries in juveniles. *The Journal of Bone and Joint Surgery. British Volume*, 56-B(3), 513-519.

- Azarnoosh, M., Stoffel, M., Quack, V., Betsch, M., Rath, B., Tingart, M., & Markert, B. (2017). A comparative study of mechanical properties of fresh and frozen-thawed porcine intervertebral discs in a bioreactor environment. *Journal of the Mechanical Behavior of Biomedical Materials*, *69*, 169-177.
- Beckstein, J. C., Sen, S., Schaer, T. P., Vresilovic, E. J., & Elliott, D. M. (2008). Comparison of animal discs used in disc research to human lumbar disc: Axial compression mechanics and glycosaminoglycan content. *Spine*, *33*(6), E166–E173.
- Brown, S. H., Gregory, D. E., & McGill, S. M. (2008). Vertebral end-plate fractures as a result of high rate pressure loading in the nucleus of the young adult porcine spine. *Journal of Biomechanics*, *41*(1), 122-127.
- Bruehlmann, S. B., Rattner, J. B., Matyas, J. R., & Duncan, N. A. (2002). Regional variations in the cellular matrix of the annulus fibrosus of the intervertebral disc. *Journal of Anatomy*, *201*(2), 159–171.
- Busscher, I., Ploegmakers, J. J. W., Verkerke, G. J., & Veldhuizen, A. G. (2010). Comparative anatomical dimensions of the complete human and porcine spine. *European Spine Journal*, *19*(7), 1104–1114.
- Cassinelli, E. H., & Kang, J. D. (2000). Current understanding of lumbar disc degeneration. *Operative Techniques in Orthopaedics*, *10*(4), 254–262.
- Chambers, N. C., Herod, T. W., & Veres, S. P. (2018). Ultrastructure of tendon rupture depends on strain rate and tendon type. *Journal of Orthopaedic Research*, *36*(11), 2842-2850.

## ENDPLATE FRACTURE

- Cheung, K. M. C. M., Karppinen, J., Chan, D., Ho, D. W. H., Song, Y.-Q., Sham, P., Luk, K. D. K. Mc. (2009). Prevalence and pattern of lumbar magnetic resonance imaging changes in a population study of one thousand forty-three individuals. *Spine*, 34(9), 934–940.
- Clemmer, J., Liao, J., Davis, D., Horstemeyer, M. F., & Williams, L. N. (2010). A mechanistic study for strain rate sensitivity of rabbit patellar tendon. *Journal of Biomechanics*, 43(14), 2785–2791.
- Costi, J. J., Freeman, B. J., & Elliott, D. M. (2011). Intervertebral disc properties: challenges for biodevices. *Expert Review of Medical Devices*, 8(3), 357-376.
- Dagenais, S., Caro, J., & Haldeman, S. (2008). A systematic review of low back pain cost of illness studies in the United States and internationally. *The Spine Journal*, 8(1), 8-20.
- Dhillon, N., Bass, E. C., & Lotz, J. C. (2001). Effect of frozen storage on the creep behavior of human intervertebral discs. *Spine*, 26(8), 883-888.
- Di Martino, A., Vaccaro, A. R., Lee, J. Y., Denaro, V., & Lim, M. R. (2005). Nucleus pulposus replacement: basic science and indications for clinical use. *Spine*, 30(16S), S16-S22.
- Dudli, S., Haschtmann, D., & Ferguson, S. J. (2012). Fracture of the vertebral endplates, but not equienergetic impact load, promotes disc degeneration in vitro. *Journal of Orthopaedic Research*, 30(5), 809–816.
- Elliott, D. M. (1999). *The fiber-induced anisotropic material behaviors of the annulus fibrosus of the intervertebral disc in tension* (Ph.D.). Duke University, United States -- North Carolina.
- Fan, S., Ghista, D., Sridhar, I., & Ramakrishna, K. (2005). Biomechanics of the intrinsically optimal design of the intervertebral disc. *Conference Proceedings: Annual International Conference of*

## ENDPLATE FRACTURE

*the IEEE Engineering in Medicine and Biology Society. IEEE Engineering in Medicine and Biology Society. Annual Conference, 4, 4408–4411.*

Farrell, M. D., & Riches, P. E. (2012). The Poisson's ratio of the nucleus pulposus is strain dependent. *Journal of Biomechanics, 45*, S566–S566.

Fields, A. J., Ballatori, A., Liebenberg, E. C., & Lotz, J. C. (2018). Contribution of the Endplates to Disc Degeneration. *Current Molecular Biology Reports, 4*(4), 151–160.

Fields, A. J., Lee, G. L., Liu, X. S., Jekir, M. G., Guo, X. E., & Keaveny, T. M. (2011). Influence of vertical trabeculae on the compressive strength of the human vertebra. *Journal of Bone and Mineral Research, 26*(2), 263–269.

Fujita Y., Wagner, D. R., Biviji, A. A., Duncan, N. A., & Lotz, J. C. (2000). Anisotropic shear behavior of the annulus fibrosus: Effect of harvest site and tissue prestrain. *Medical Engineering and Physics, 22*(5), 349–357.

Gregory, D. E., Bae, W. C., Sah, R. L., & Masuda, K. (2014). Disc degeneration reduces the delamination strength of the annulus fibrosus in the rabbit annular disc puncture model. *The Spine Journal, 14*(7), 1265–1271.

Gregory, D. E., Veldhuis, J. H., Horst, C., Wayne Brodland, G., & Callaghan, J. P. (2011). Novel lap test determines the mechanics of delamination between annular lamellae of the intervertebral disc. *Journal of Biomechanics, 44*(1), 97–102.

- Gregory, D. E. (2009). The influence of the tensile material properties of single annulus fibrosus lamellae and the interlamellar matrix strength on disc herniation and progression (unpublished doctoral dissertation). University of Waterloo, Waterloo, Ontario, Canada.
- Hadjipavlou, A. G., Tzermiadianos, M. N., Bogduk, N., & Zindrick, M. R. (2008). The pathophysiology of disc degeneration. *The Journal of Bone and Joint Surgery. British Volume, 90-B(10)*, 1261–1270.
- Harrison, R. A., Siminoski, K., Vethanayagam, D., & Majumdar, S. R. (2007). Osteoporosis-Related Kyphosis and Impairments in Pulmonary Function: A Systematic Review. *Journal of Bone and Mineral Research, 22(3)*, 447–457.
- Harvey-Burgess, M., & Gregory, D. E. (2018). The Effect of Axial Torsion on the Mechanical Properties of the Annulus Fibrosus. *Spine*.
- Jung, H.-J., Fisher, M. B., & Woo, S. L.-Y. (2009). Role of biomechanics in the understanding of normal, injured, and healing ligaments and tendons. *Sports Medicine, Arthroscopy, Rehabilitation, Therapy, and Technology : SMARTT, 1*, 9–9.
- Karlsson, L., Lundin, O., Ekström, L., Hansson, T., & Sward, L. (1998). Injuries in adolescent spine exposed to compressive loads: An experimental cadaveric study. *Journal of Spinal Disorders, 11(6)*, 501–507.
- Li, J., Liu, C., Guo, Q., Yang, H., & Li, B. (2014). Regional variations in the cellular, biochemical, and biomechanical characteristics of rabbit annulus fibrosus. *PLoS ONE, 9(3)*.

- Lundin, O., Ekström, L., Hellström, M., Holm, S., & Sward, L. (2000). Exposure of the porcine spine to mechanical compression: Differences in injury pattern between adolescents and adults. *European Spine Journal*, 9(6), 466–471.
- Lundin, O., Ekstrom, L., Hellstrom, M., Holm, S., & Sward, L. (1998). Injuries in the adolescent porcine spine exposed to mechanical compression. *Spine*, 23(23), 2574–2579.
- Malko, J. A., Hutton, W. C., & Fajman, W. A. (1999). An in vivo magnetic resonance imaging study of changes in the volume (and fluid content) of the lumbar intervertebral discs during a simulated diurnal load cycle. *Spine*, 24(10), 1015-1022.
- Mehrkens, A., Müller, A. M., Valderrabano, V., Schären, S., & Vavken, P. (2012). Tissue engineering approaches to degenerative disc disease – A meta-analysis of controlled animal trials. *Osteoarthritis and Cartilage*.
- Melrose, J., Smith, S. M., Appleyard, R. C., & Little, C. B. (2008). Aggrecan, versican and type VI collagen are components of annular translamellar crossbridges in the intervertebral disc. *European Spine Journal*, 17(2), 314–324.
- Monaco, L. A., DeWitte-Orr, S. J., & Gregory, D. E. (2016). A comparison between porcine, ovine, and bovine intervertebral disc anatomy and single lamella annulus fibrosus tensile properties. *Journal of Morphology*, 277(2), 244–251.
- Murakami, H., Yoon, T., Attallah-Wasif, E., Kraiwattanapong, C., Kikkawa, I., & Hutton, W. (2010). Quantitative differences in intervertebral disc–matrix composition with age-related degeneration. *Medical & Biological Engineering & Computing*, 48(5), 469–474.

## ENDPLATE FRACTURE

- O'Connell, G. D. B., Vresilovic, E. J., & Elliott, D. M. (2007). Comparison of animals used in disc research to human lumbar disc geometry. *Spine*, *32*(3), 328–333.
- Oxland, T. R., Panjabi, M. M., Southern, E. P., & Duranceau, J. S. (1991). An anatomic basis for spinal instability: a porcine trauma model. *Journal of Orthopaedic Research*, *9*(3), 452-462.
- Przybyla, A., Pollintine, P., Bedzinski, R., & Adams, M. A. (2006). Outer annulus tears have less effect than endplate fracture on stress distributions inside intervertebral discs: Relevance to disc degeneration. *Clinical Biomechanics*, *21*(10), 1013–1019.
- Pye, S. R., Reid, D. M., Lunt, M., Adams, J. E., Silman, A. J., & O'neill, T. W. (2007). Lumbar disc degeneration: association between osteophytes, end-plate sclerosis and disc space narrowing. *Annals of the Rheumatic Diseases*, *66*(3), 330-333.
- Rao, A. A., & Dumas, G. A. (1991). Influence of material properties on the mechanical behaviour of the L5-S1 intervertebral disc in compression: a nonlinear finite element study. *Journal of Biomedical Engineering*, *13*(2), 139-151.
- Rapoport, J., Jacobs, P., Bell, N. R., & Klarenbach, S. (2004). Refining the measurement of the economic burden of chronic diseases in Canada. *Age*, *20*(39), 1-643.
- Renau, A., Farrerons, J., Yoldi, B., Gil, J., Proubasta, I., Llauger, J., & Planell, J. (2004). Yield point in prediction of compressive behavior of lumbar vertebral body by dual-energy X-ray absorptiometry. *Journal of Clinical Densitometry*, *7*(4), 382-389.

- Rodriguez, A. G., Rodriguez-Soto, A. E., Burghardt, A. J., Berven, S., Majumdar, S., & Lotz, J. C. (2012). Morphology of the human vertebral endplate. *Journal of Orthopaedic Research*, 30(2), 280-287.
- Rodrigues, S. A., Thambyah, A., & Broom, N. D. (2017). How maturity influences annulus-endplate integration in the ovine intervertebral disc: A micro- and ultra-structural study. *Journal of Anatomy*, 230(1), 152–164.
- Roughley, P. J., Alini, M., & Antoniou, J. (2002). The role of proteoglycans in aging, degeneration and repair of the intervertebral disc.
- Setton, L. A., & Chen, J. (2004). Cell mechanics and mechanobiology in the intervertebral Disc. *Spine*, 29(23), 2710–2723.
- Showalter, B. L. B., Beckstein, J. C. M., Martin, J. T. M., Beattie, E. E., Orias, A. A. E., Schaer, T. P. V., Elliott, D. M. (2012). Comparison of animal discs used in disc research to human lumbar disc: Torsion mechanics and collagen content. *Spine*, 37(15).
- Snow, C. R., Harvey-Burgess, M., Laird, B., Brown, S. H., & Gregory, D. E. (2018). Pressure-induced end-plate fracture in the porcine spine: Is the annulus fibrosus susceptible to damage?. *European Spine Journal*, 27(8), 1767-1774.
- Stokes, I. A., & Iatridis, J. C. (2004). Mechanical conditions that accelerate intervertebral disc degeneration: overload versus immobilization. *Spine*, 29(23), 2724-2732.
- Vos, T., Flaxman, A. D., Naghavi, M., Lozano, R., Michaud, C., Ezzati, M., & Abraham, J. (2012). Years lived with disability (YLDs) for 1160 sequelae of 289 diseases and injuries 1990–2010: a

systematic analysis for the Global Burden of Disease Study 2010. *The Lancet*, 380(9859), 2163-2196.

Weiss, J. A., Gardiner, J. C., & Bonifasi-Lista, C. (2002). Ligament material behavior is nonlinear, viscoelastic and rate-independent under shear loading. *Journal of Biomechanics*, 35(7), 943–950.

Yingling, V. R., Callaghan, J. P., & McGill, S. M. (1999). The porcine cervical spine as a model of the human lumbar spine: an anatomical, geometric, and functional comparison. *Journal of Spinal Disorders*, 12(5), 415-423.